2
Literature Review

This section of the thesis looks into the early research conducted on lightweight aluminium alloys, focusing on the significant contributions of Al-Si alloys. The importance of this research is underscored by the nature of two-phase alloys, their deformation behaviour, their mechanical properties, and their mutual relationships. This chapter offers a comprehensive overview of the research that investigated the effect of various processing on the microstructure evolution and flow behaviour of Al-Si alloys at ambient and elevated temperatures. It encompasses the microstructural modifications by chemical, thermal, and mechanical means and their impact on mechanical properties. The microstructural changes resulting from conventional and severe plastic deformation of Al-Si alloys are discussed. Furthermore, a meticulous literature survey on the deformation behaviour of the two-phase alloys at ambient and elevated temperatures has been conducted and is presented in this chapter. Additionally, the effects of composition and process on microstructure, mechanical property, and their inter-relationships, as reported in the literature, have been discussed.

2.1 IMPORTANCE OF PURE Al AND Si

As we know, the ores of aluminium and silicon are easily available elements in the Earth's crust (Davis, 1993). A pie chart of the elements is presented in Figure 2.1 (Earle, 2015), which is available in the Earth's crust. Although extracting pure Al from the ore is much more costly, its exceptional properties, such as conductivity, corrosion resistance, and high specific strength, make it more viable for various applications. Thus, the production of Al is very necessary for every country. Al is used extensively in a range of industries, including aerospace, automotive, construction, and packaging (C.Robles-Hernandez and Jose Martin Herrera Ramirez, 2017; Godbole *et al.*, 2024). On the other hand, silicon is hard (Mohs hardness = 6.5), lightweight (2.3g/cc), and brittle in nature. Silicon holds critical importance in the electronics industry as the fundamental component of semiconductors, essential for manufacturing integrated circuits, microchips, and photovoltaic cells (Green, 2000; Stephen A. Campbell, 2001; S. M. Sze and Kwok K. Ng, 2007). Additionally, silicon plays a significant role in alloys and ceramics, and as a dopant in producing silicon-based materials for a wide range of applications. The physical and mechanical properties of both elements are listed in Table 2.1. It is clear from Table 2.1 that the properties of pure Al or pure Si are insufficient independently to fulfil the demand of the specific application. The combination of two abundantly available elements, Al and Si, with comparative densities, but widely different mechanical properties provide an opportunity to produce a material with physical properties ranging from that of pure Al to pure Si, with the intermediate phases of the solid solution of Si in Al, and hypoeutectic to hypereutectic phases. Si is the most important alloying element for pure Al to get the desired properties in the form of aluminium-silicon (Al-Si) alloys. It increases the fluidity of the Al-Si alloys and reduces the casting defects. Al-Si alloys are categorized into non-heat-treatable cast alloys, Figure 2.2.

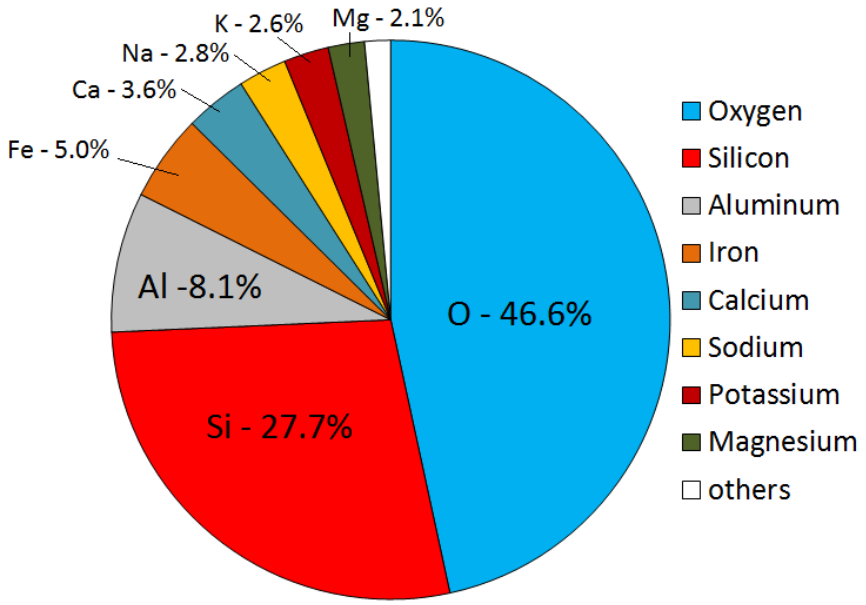


Figure. 2.1 : A pie chart distribution of the elements (mass%) in the Earth's crust (*Source*: Steven Earle, 2015)

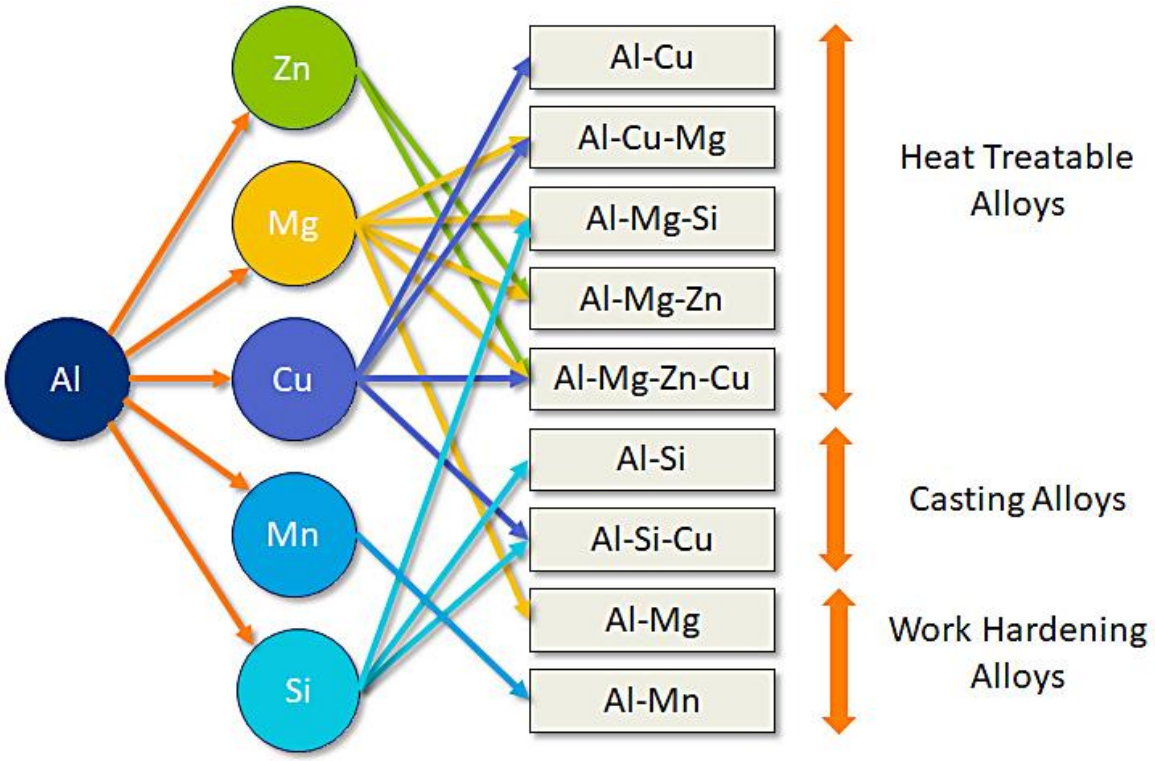


Figure. 2.2 : Aluminium alloy classification based on alloying elements and alloy type (*Source*: Davis, 1993; J. Zhang et al., 2019)

Table 2.1 : The physio-mechanical properties of pure Al and Si (*Source*: Davis, 1993)

Physical Properties			*Mechanical Properties*		
	Al	Si		Al	Si
Melting Point (K)	933	1687	Yield Strength (MPa)	30	165
Density (g/cc)	2.7	2.3	Tensile strength (MPa)	91.5	170
Resistivity (mΩ)	2.6×10^{-8}	1×10^{-3}	Elongation (%)	30.1	-
Thermal conductivity (W/mK)	235	150	Young's Modulus (GPa)	70	165
Coefficient of thermal expansion (K^{-1})	23.1×10^{-6}	2.6×10^{-6}	Hardness (HV)	57.98	700-1000

2.2 PROCESSING METHODS OF Al-Si ALLOYS

Based on the Al-Si alloy phase diagram, Figure 2.3, and the silicon content, Al-Si alloys are categorized into three groups: (i) when the silicon content is less than 12.6wt.%, it is referred to as hypoeutectic Al-Si alloy; (ii) at approximately 12.6wt.% silicon content, it is termed as eutectic Al-Si alloy; and (iii) if silicon content exceeds 12.6wt.%, it is considered a hypereutectic Al-Si alloy. Various fabrication techniques can be employed to produce Al-Si alloy, including melting and casting, powder metallurgy, spray forming, and additive manufacturing (Davis, 1993; C. Cui *et al.*, 2009; Richter, Sajadifar and Niendorf, 2021; Liu *et al.*, 2022).

The melting and casting process of Al-Si alloy has undergone gradual advancements and refinements over many years. However, it gained significant attention and development during the early to mid-20th century, coinciding with the increasing importance of aluminium across various industries. This process has served as a primary method for producing Al-Si alloys since as far back as 1920. The addition of silicon enhances the fluidity of the alloy, facilitating defect-free casting. Currently, more than 80% of worldwide as-cast aluminium alloys fall under the category of Al-Si alloys (Małgorzata Warmuzek, 2004). Other alloying elements can be incorporated during the melting and casting process to strengthen the alloys, along with potential impacts on mechanical properties. Iron (Fe) emerges as the primary impurity in as-cast Al-Si alloys due to the commercial purity of aluminium and silicon, which varies based on silicon content (Taylor, 2012). Fe can originate from various sources, including the furnace equipment and the stirring rod, as Taylor et al. (Taylor, 2012) observed. Investigations by Tiedje, Bolibruchova and Matejka, and Kasinska *et al*. have explored the relationship between Fe and Si content, noting the formation of the Al5FeSi intermetallic compound at critical levels of Fe content prior to Al-Si eutectic formation, depending on temperature (Tiedje, Taylor and Easton, 2012; Dana Bolibruchová, 2019; Kasińska, Bolibruchová and Matejka, 2020). The melting and casting of Al-Si alloy predominantly focus on eutectic compositions because of the challenges associated with producing hypereutectic compositions owing to the low solubility of Si in Al. Additionally, the as-cast hypereutectic Al-Si alloys typically exhibit poor mechanical properties due to the coarse and non-homogeneous distribution of the silicon particles.

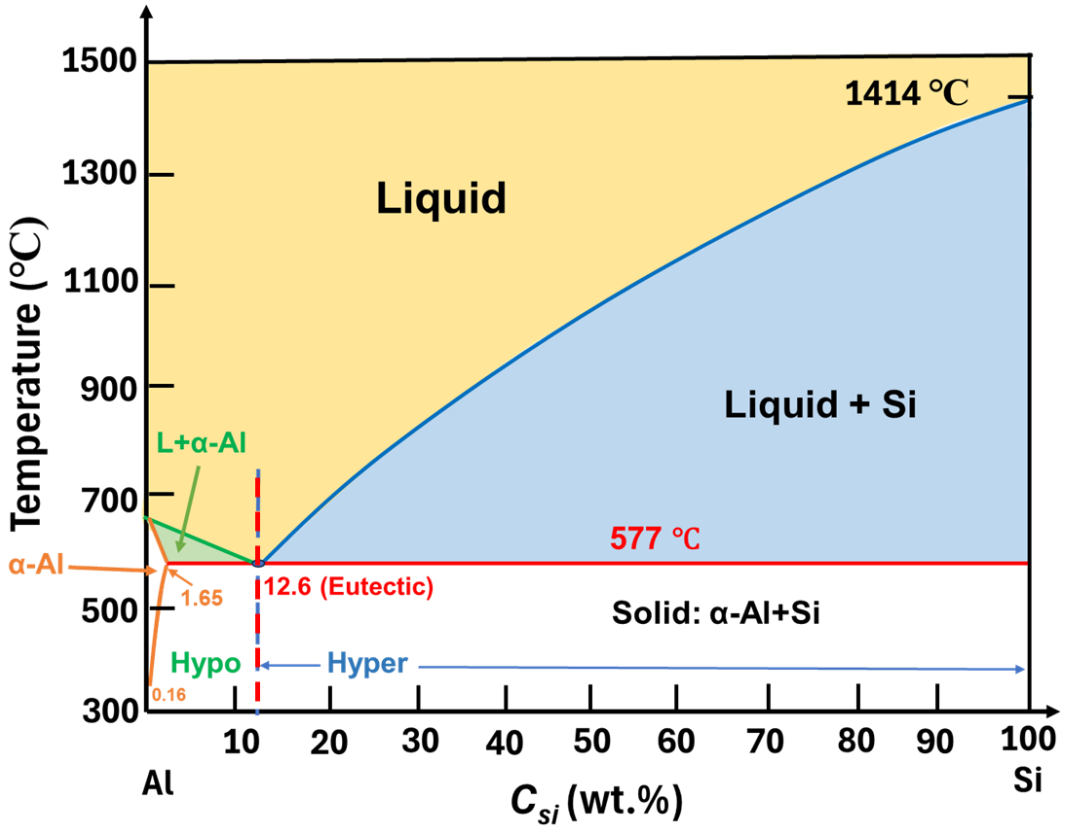


Figure 2.3 : Schematic phase diagram of Al-Si alloy showing the classification of compositions by the vertical dotted line (*Source*: Murray and McAlister, 1984)

To overcome the limitations of the melting process and resulting mechanical properties, alternative techniques such as powder metallurgy, spray forming, and additive manufacturing have been developed to enhance the mechanical properties and expand the range of silicon content in Al-Si alloy compositions by refining the microstructure. Powder metallurgy has a long history of producing complex, near-net-shaped parts of Al-Si alloys (Donald G. White, 1998), while spray forming and additive manufacturing represent newer approaches (C. Cui *et al.*, 2009; Richter, Sajadifar and Niendorf, 2021; Liu *et al.*, 2022). These methods offer the advantage of producing Al-Si alloys with silicon contents exceeding 50wt.%, presenting a potential alternative to Bakelite in electronic packaging applications (Kun *et al.*, 2008; Haque *et al.*, 2018; Godbole *et al.*, 2024). The emergence of powder metallurgy aluminium alloys was highlighted as early as the 1930s, as noted by Haertlein and Sachse during the Metal Powder Association's ninth annual meeting in 1953 (Takeda *et al.*, 1990). LaDelpha *et al.* demonstrated the viability of powder metallurgy technology in replicating the properties of AA4032-T651 alloy, achieving comparable tensile properties, hardness, and aging response (LaDelpha *et al.*, 2008). Yamauchi *et al.* further expanded the scope by producing Al-Si alloys with silicon content ranging from 7.1% to 23.7% using the powder metallurgy route (Yamauchi *et al.*, 1985).

The spray-forming process, pioneered in the late 1980s, specifically in 1987, by Atakan Peker and Gary E. Fuchs at the National Institute of Standards and Technology (NIST) in the United States, involves spraying molten metal or alloy onto a substrate. This rapid cooling and solidification process results in the formation of dense components. Spray forming has proven to be effective in producing hypereutectic Al-Si alloys with high silicon content, characterized by refined and uniformly distributed primary silicon and modified eutectic structures. Cui *et al.* successfully developed high silicon content Al-18Si, Al-25Si, and Al-35Si hypereutectic alloys using the spray-forming process, leading to finely distributed primary silicon and altered eutectic structures (Chengsong Cui *et al.*, 2009; Cui *et al.*, 2010). They further investigated the deformation behaviour of these alloys. Similarly, Hogg *et al.* explored the impact of

solidification conditions on the microstructural variation of spray-formed Al-30Si hypereutectic alloy (Hogg *et al.*, 2006). Satoh *et al*. reported that rapid-solidification-processed hypereutectic Al-Si powder metallurgy alloys exhibited superplastic-like behaviour, achieving maximum elongations of 154% and 307% at temperatures just below their solidus temperatures (Satoh, Okimoto, S. Nishida, *et al.*, 1995). Another study by Kim *et al*. investigated that spray-deposited Al-25Si alloy demonstrated superplastic behaviour at elevated temperatures due to the aluminium matrix, with significant whisker formation attributed to the liquidation of grain boundary and its sliding during deformation (W. Kim, Yeon and Lee, 2000).

The additive manufacturing (AM) of Al-Si alloy has been developed over several years through ongoing research and advancements in materials science and AM technology. Research and development in this area have been ongoing since the early 2000s, with notable advancements and publications occurring in subsequent years (Peng *et al.*, 2018; Aversa *et al.*, 2019; Ruano *et al.*, 2019; Jia *et al.*, 2020; Vafadar *et al.*, 2021; Luo, Sachdev and Apelian, 2022). Additive manufacturing of Al-Si alloys continues to be an active area of research and development, with new techniques, materials, and applications being explored. Al-Si alloys can be fabricated by using different processing techniques, as illustrated in Figure 2.4 (Dash and Chen, 2023).

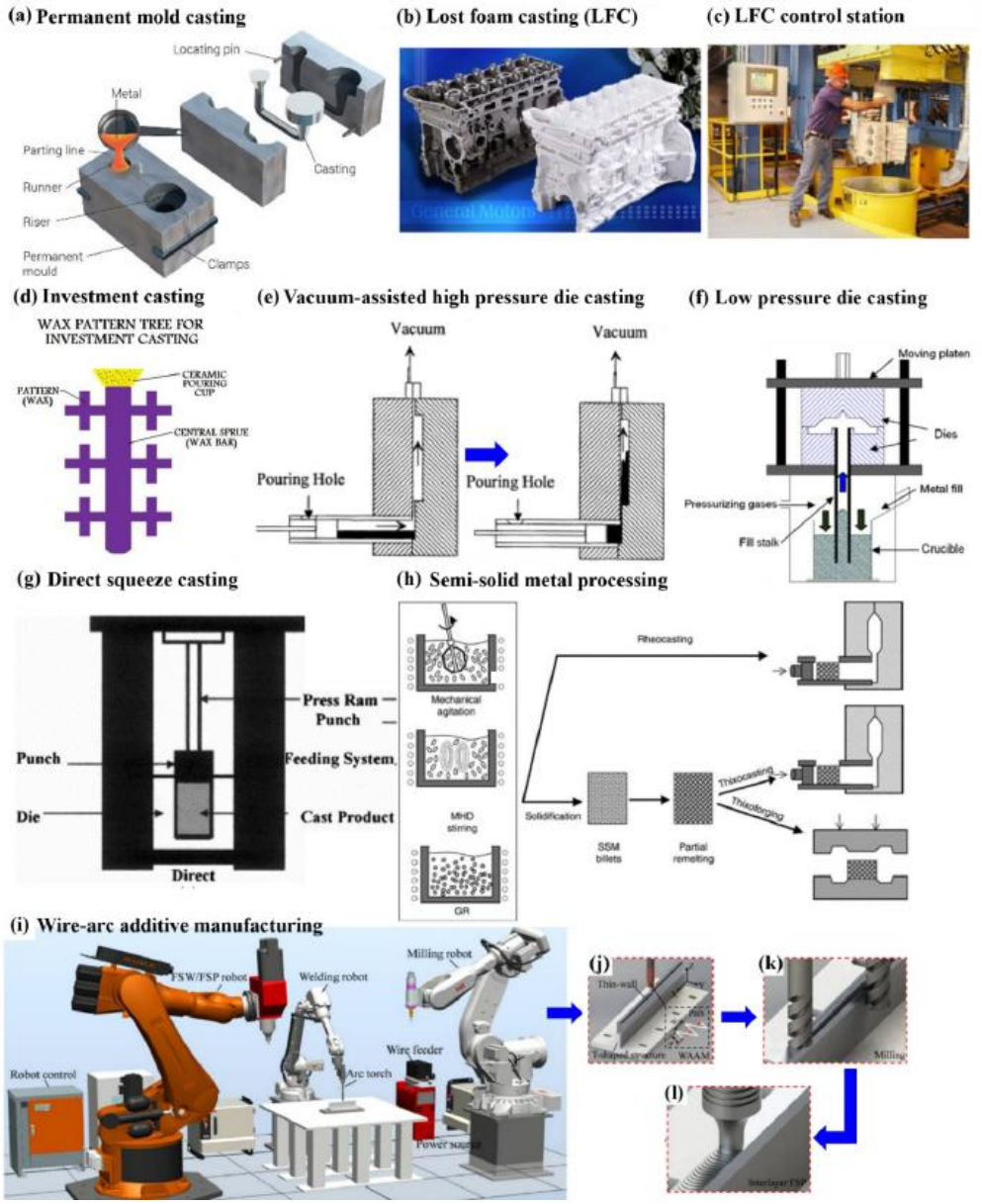


Figure. 2.4 : Schematic illustration of different methods to fabricate the Al-Si alloys (*Source*: Dash and Chen, 2023)

2.3 MICROSTRUCTURAL EVOLUTION UNDER DIFFERENT PROCESSING CONDITIONS

2.3.1 Microstructure Evolution during Melting and Casting

Solidification steps in Al-Si alloys

During the solidification process of hypoeutectic Al-Si alloys, the FCC-Al solid phase initiates growth from the liquid (FCC-Al + Liquid) at the liquidus temperature. Subsequently, the remaining liquid transforms into the eutectic mixture (FCC-Al + Diamond cubic Si) of fine Al and silicon forms at the solidus temperature of 850K, where the solidification ends. Consequently, at room temperature, the microstructure of hypoeutectic Al-Si alloy comprises a dendritic FCC-Al matrix surrounded by a fine mixture of Al and Si eutectic phase within a two-phase field. The emergence of fine silicon from the supersaturated FCC-Al solid solution is facilitated by the low solubility (<0.05wt.%) of Si in Al at room temperature (Mostafa and Alshabatat, 2022). Conversely, for hypereutectic Al-Si alloys, the nucleation of primary Si (diamond cubic) precedes the growth of FCC-Al grain and eutectic phase sequentially. Cui *et al*. conducted calculations of solid-liquid phase fractions, enthalpy, and other thermochemical data as a function of temperature using Thermo-Calc software (C. Cui *et al*., 2009). Ferreira *et al*. investigated the solidification behaviour of hypoeutectic Al-3Si and Al-5Si alloys (Sales *et al*., 2018), while Xu *et al*. investigated the formation kinetics of primary Si particles during the solidification of hypereutectic Al-Si alloy using the micro-focus *in situ* X-radiography method (Xu *et al*., 2020).

Hypoeutectic Al-Si alloys

$$\text{Liquid} \longrightarrow \text{Liquid} + \text{FCC-Al} \longrightarrow \text{FCC-Al} + \text{Diamond Si}$$

Hypereutectic Al-Si alloys

$$\text{Liquid} \longrightarrow \text{Liquid} + \text{Diamond Si} \longrightarrow \text{FCC-Al} + \text{Diamond Si}$$

The microstructure of the Al-Si alloy at room temperature consists of three phase components: (i) α-Al as a major constituent, which is known to be the matrix phase, (ii) a fine eutectic mixture of Al and Si, and (iii) primary Si particles. In as-cast hypoeutectic Al-Si (Si<12.6wt.%) alloys, the α-Al phase forms in a dendritic shape along with the fine eutectic mixture, whereas coarse primary Si particles are present in hypereutectic Al-Si (Si>12.6wt.%) alloys. The morphologies and volume fraction of phases depend upon the solidification conditions and chemical composition in the Al-Si alloys. Many authors reported the effect of the cooling rate (Haque and Maleque, 1998; Kang *et al*., 2010; Riestra *et al*., 2017; Shen *et al*., 2022; Mao *et al*., 2023; Zhu *et al*., 2023), and studied the effect of Si content on grain size, secondary dendrite arm spacing (SDAS), and primary Si size (Xu and Jiang, 2006; Birol, 2012; Sales *et al*., 2018). From the previous studies (Kobayashi, Shingu and Ozaki, 1975; Lu and Hellawell, 1985; Wang, Lu and Hogan, 1999; Xu *et al*., 2006; L. Zhang *et al*., 2020) It is stated that the primary Si particles can be formed in various morphologies like plate-type, star-like, polyhedral (octahedral) shape, feathery silicon, dendritic primary silicon, and spheroidal primary silicon (Vijeesh and Prabhu, 2014), as shown in Figure 2.5. The Si has a diamond cubic structure, which promotes its growth in a faceted manner in {111} planes by the twin plane re-entrant angle (TPRE) mechanism (Lu and Hellawell, 1985). In the TPRE growth mechanism, the twin crystal surface facilitates maintaining the stable groove for the growth of Si in a specific direction <112> with a twin plane of {111}.

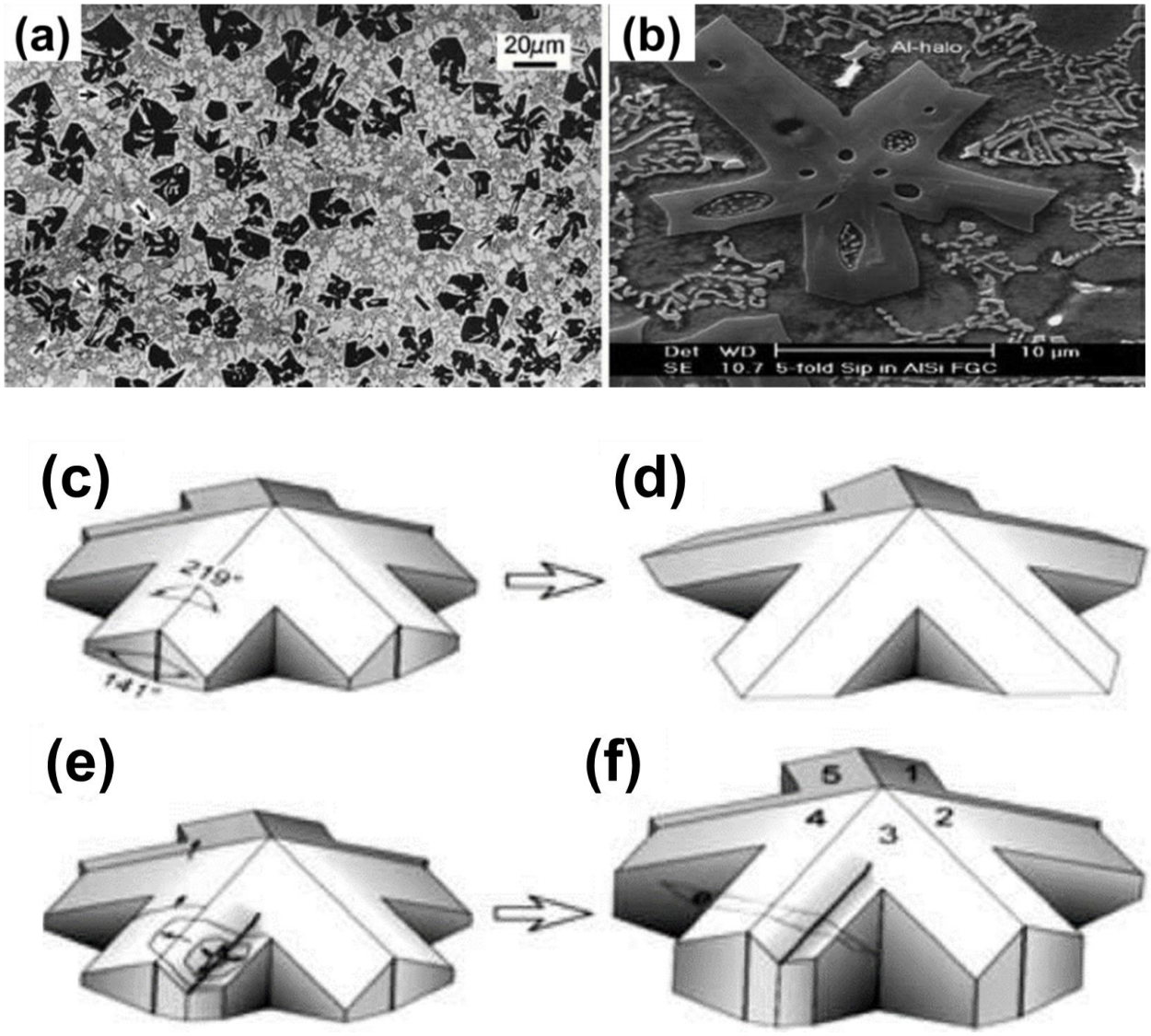


Figure. 2.5 : Microstructure of as-cast Al-Si alloy having different morphologies: (a) plate type, (b) star type (five-fold) shape, and (c-f) Schematic figure of fivefold growth of primary Si particles (*Source*: Vijeesh and Prabhu, 2014)

In the as-cast microstructure, the coarse and inhomogeneous distribution of Si particles plays an adverse role in the degradation of the mechanical properties of Al-Si alloys. Also, hypereutectic Al-Si alloy is a hard-to-work material because the matrix and particles show incompatibility during plastic deformation, which results in low deformability. The mechanical properties of the as-cast alloy are affected by microstructural aspects, mainly that of the Si particles. The morphology of the Si particles can be altered by chemical modification (Qiyang, Qingchun and Qifu, 1991), thermal treatment (Haque and Maleque, 1998; Kang *et al.*, 2010; Riestra *et al.*, 2017; Shen *et al.*, 2022; Mao *et al.*, 2023; Zhu *et al.*, 2023), and by using mechanical working (Harris, 1983; Guiglionda and Poole, 2002; Zhilyaev *et al.*, 2007; Ke *et al.*, 2010; Meenia *et al.*, 2016; Jin *et al.*, 2021). These methods are elaborated with the help of previously reported studies under the next subheading.

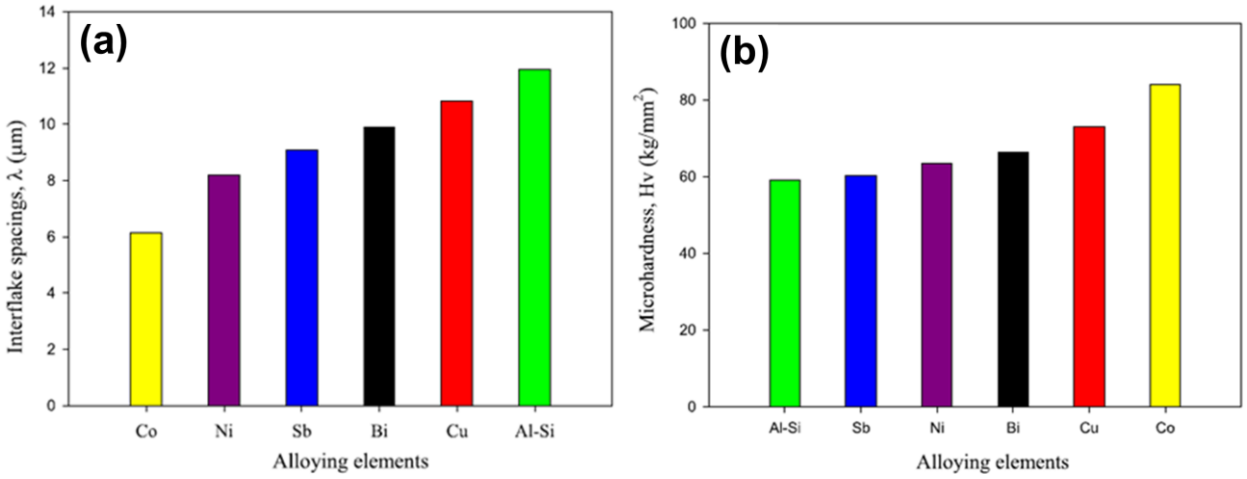
2.3.2 Microstructure Refinement/Modification Techniques

Microstructure refinement or modification is required to reduce the casting defects and improve the properties in the as-cast state of the materials. Chemical modification is one of the common methods used by industries to refine cast aluminium alloys. According to previous studies (Shamsuzzoha and Hogan, 1986; Qiyang, Qingchun and Qifu, 1991; Ogris *et al.*, 2002; Li *et al.*, 2015; Barrirero *et al.*, 2016), Na, P, Sr, K, Sc, Ca, and B can be introduced as metallic elements that are used in small proportions to modify the coarse Si particles into fine spheroidal

particles in Al-Si alloys. The microstructure containing fine Si improves the deformability and strength of alloys. Moniri and Shahani reported a survey on the effect of chemical modification on microstructural refinement and mechanical properties (Moniri and Shahani, 2019). Barrirero *et al*. investigated the effect of Na and Sr on the eutectic modification of Si and the resulting mechanical properties (Barrirero *et al*., 2016). In another study, Gursoy *et al*. studied the effect of lanthanides as trace elements for chemical modification of the as-cast microstructure. They stated that it could be an alternative to the Na, Sr modifier for eutectic modification of Si in hypoeutectic Al-Si cast alloy (Gursoy and Timelli, 2020). Ding *et al*. reported the modification of Si particles from coarse plate-like shape to fine globular structure by a novel Al-3Ti-4.35La master alloy, which enhances elongation by more than 100% (Wanwu Ding, Lumin Gou, Haixia Zhang, Wenjun Zhao, Jinyuan Ma, Jisen Qiao, 2022). In an interesting study, Barrirero *et al*. investigated the influence of rare earth elements Eu and Yb on the microstructure and reported that the eutectic microstructure converted into a coral-like structure (Barrirero *et al*., 2019). Jiang *et al*. proposed 0.5% Al-15La and 0.5% Mg-15La as novel modifiers for refining the eutectic Si and reported the enhancement caused by them in mechanical properties (Bo Jiang, Zesheng Ji, Maoliang Hu, Hongyu Xu, 2019).

However, the thermal treatment method basically belongs to the melting and solidification conditions of the alloy. The refinement can be done by rapid cooling and some other ways of heat treatment. In most of the studies, both of the above modification techniques have been used to refine the eutectic Si to some extent. Thus, it can be used up to eutectic composition (Si≤12.6wt.%), where the Si size is small, not for hypereutectic Al-Si alloys, which contain very large size Si particles (Primary Si). Apart from that, the addition of elements leads to changes in the chemical composition of the alloy, which may produce casting defects (porosity, shrinkage, cracks). These microstructural inhomogeneities deteriorate the mechanical properties.

Kaya and Aker reported the effect of alloying elements on the microstructural features and mechanical properties of the alloys, as presented in Figure 2.6 (Kaya and Aker, 2017).



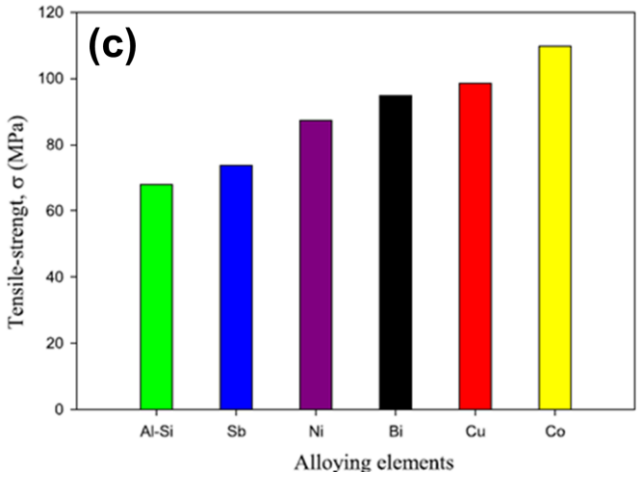


Figure. 2.6 : Variation in interparticle spacing (a), microhardness (b), and tensile strength (c) as a function of alloying elements in Al-Si alloy (*Source*: Kaya and Aker, 2017)

The above methods could not be applied to get an ultra-fine grain (UFG) microstructure. To overcome this limitation, different mechanical processing such as extrusion, rolling, forging, and severe plastic deformation (SPD) like friction stir processing (FSP), equal channel angular pressing (ECAP), high-pressure torsion (HPT), and accumulative roll bonding (ARB) were used. A detailed explanation of these techniques used for different purposes in different types of metals and alloys is presented in the next level subheadings of this chapter.

(a) Mechanical Working

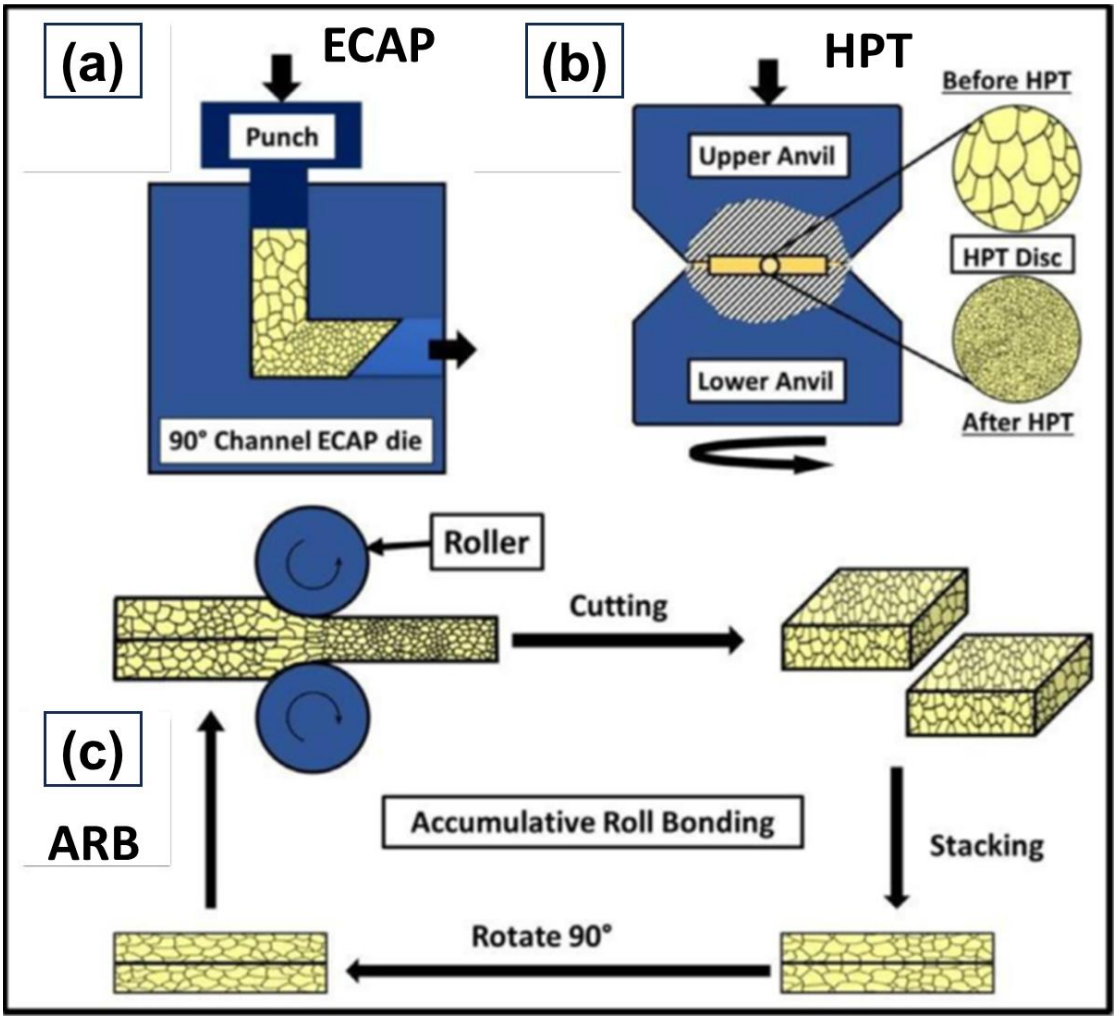
Mechanical working can be divided into conventional processing and severe plastic deformation (SPD) to refine the microstructure and enhance the mechanical properties of Al alloys (Guan and Tie, 2017). Conventional mechanical processing involves the plastic deformation of the material, which leads to breaking the coarse as-cast structure into fine grains and a homogeneous distribution of the particles, promoting material strengthening. It applies to a wide range of Al alloys, but the grain size and particle size are typically limited to approximately 5-10µm based on the reported results in the previous studies (Cui *et al.*, 2010; Ke *et al.*, 2010; Liu *et al.*, 2011; Gode *et al.*, 2014; Wang *et al.*, 2014; Wu *et al.*, 2014; Ma *et al.*, 2017; Nithin, Davidson and Rao, 2020; Sakow *et al.*, 2020; Y. Zhang *et al.*, 2020).

Cui *et al.* investigated hypereutectic Al-Si alloy produced through the extrusion process and observed well-fragmented silicon particles in 5-10µm globular shapes with homogeneous dispersion (Cui *et al.*, 2010). Similarly, Ke *et al.* reported a grain size of approximately less than 15µm after hot extrusion of Al-12Si-0.2Mg alloy (Ke *et al.*, 2010). Many more studies (Liu *et al.*, 2011; Gode *et al.*, 2014; Wang *et al.*, 2014; Wu *et al.*, 2014; Lv *et al.*, 2018; Nithin, Davidson and Rao, 2020; Sakow *et al.*, 2020; Y. Zhang *et al.*, 2020) have reported the improvement in physio-mechanical properties through the change in phase proportion, grain and particle sizes, morphological changes, and their distributions in the two-phase materials by the extrusion process. Immanuel and Panigrahi (Immanuel and Panigrahi, 2015, 2016) investigated the effect of thermo-mechanical treatment (cryo-rolling and subsequent heat treatment) on the morphology and distribution of eutectic Si particles in the as-cast Al-Si alloy (A356). The microstructural changes led to enhancing the strength (248%), ductility (37%), and tribological properties of the Al-Si alloy.

Severe Plastic Deformation (SPD)

Severe plastic deformation is a processing technique that can produce UFG material without changing the cross-sectional dimensions of the sample. It is even widely used for different metals and alloys to produce the grain size of the nanocrystalline range of <100 nm (Edalati and Horita, 2016; Segal, 2018; Edalati *et al.*, 2022), which is otherwise impossible to

generate by conventional processing. Due to large plastic strain during severe deformation, the high dislocation density introduced in the material causes sub-structure formation and homogeneity within the microstructure, leading to enhanced strength and ductility. So far, many investigations have been published to produce nanocrystalline grains of metallic, ceramic, and composite materials by applying various SPD techniques (Edalati *et al.*, 2022). It involves equal-channel angular pressing (ECAP) (Segal, 1995; Valiev and Langdon, 2006; Natori, Utsunomiya and Tanaka, 2021), high-pressure torsion (HPT) (Bridgman, 1935; Edalati and Horita, 2016; Muñoz *et al.*, 2024), accumulative roll-bonding (ARB) (Ghalehbandi, Malaki and Gupta, 2019), friction stir processing (FSP) (Mishra and Ma, 2005; Patel *et al.*, 2019), cyclic extrusion-compression (CEC) (Richert *et al.*, 2003; El-Garhy, El Mahallawy and Shoukry, 2021), multi-directional forging (MDF) (Alemdag *et al.*, 2021), repetitive corrugation and straightening (RCS) (Romero-Resendiz *et al.*, 2021), twist extrusion (TE) (Nouri *et al.*, 2018), tube cyclic extrusion-compression (TCEC) (Babaei and Mosavi Mashadi, 2014), and accumulative continuous extrusion forming (ACEF) (Wang *et al.*, 2017; Hu *et al.*, 2019). Schematic diagrams of typical SPD techniques are taken from the literature and presented in Figure 2.7.



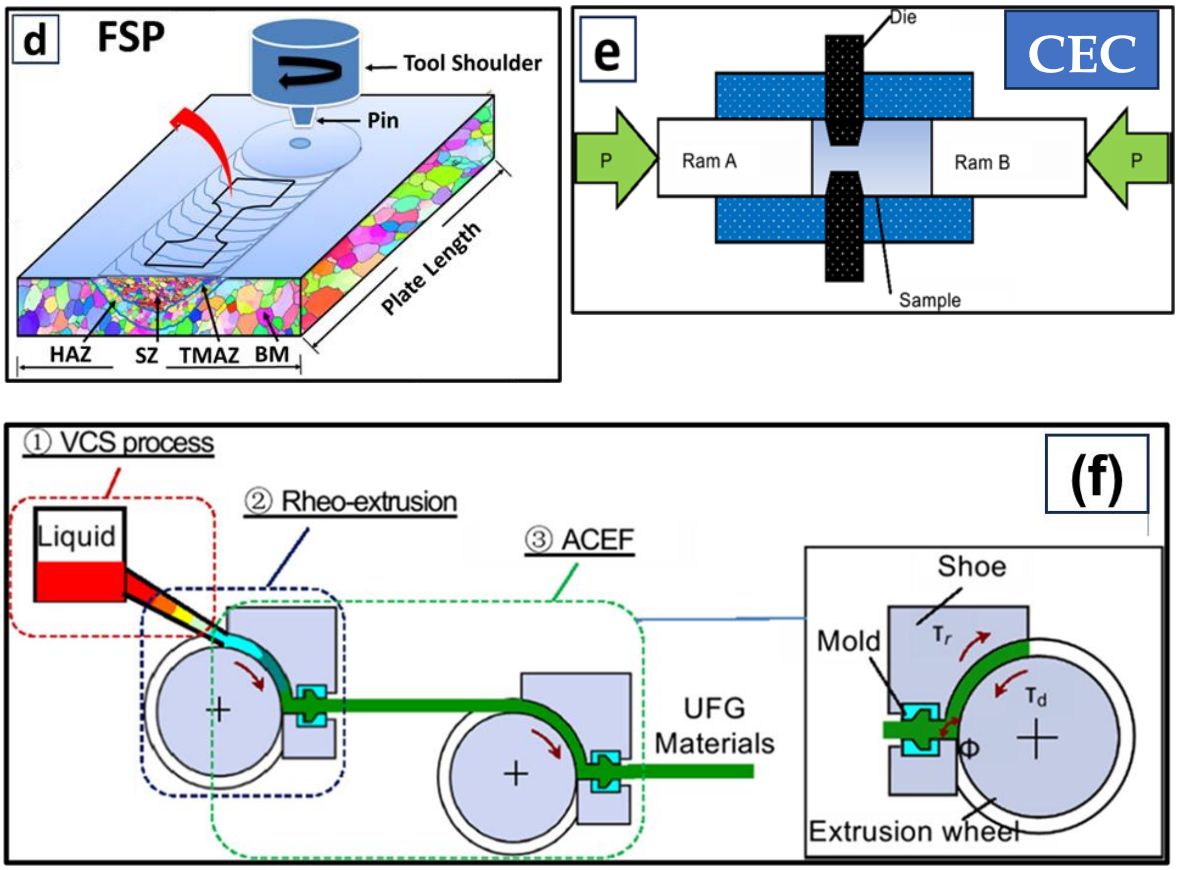


Figure. 2.7 : Schematic diagrams of typically given SPD techniques: (a) ECAP, (b) HPT, (c) ARB, (d) FSP, (e) CEC, and (f) ACEF (*Source*: Hu et al., 2019; Rakshith and Seenuvasaperumal, 2021)

Among all the SPD techniques, ECAP, HPT, ARB, and FSP have been widely investigated and well-established for producing UFG materials. ECAP was first developed as a metal-forming process by Segal (Segal, 1995), and the subsequent work on UFG microstructure through ECAP was done by Valiev *et al*. (Valiev *et al*., 1996; Valiev and Langdon, 2006). Iwahashi *et al*. reported the grain refinement in the form of elongated sub-grains of pure Al from an initial value of 1.0mm to ~1µm using the ECAP method (Iwahashi *et al*., 1997). In another study, Tolaminejad and Dehghani investigated the effect of ECAP on pure aluminium and obtained a final grain size of 0.3µm compared to the 50µm initial grain size and improved mechanical properties (Tolaminejad and Dehghani, 2012). Further, some studies have been done to investigate the effect of SPD on the two-phase materials. Purcek *et al*. reported the Si particle refinement from an initial size of ~35µm to 1.3µm after six ECAE passes of Al-Si alloy. The tensile and yield strengths were enhanced by 68% and 100%, respectively (Purcek, Saray and Kul, 2010). Yoon *et al*. applied ECAP up to eight passes to refine the matrix and the Si particles of hypereutectic Al-20Si alloy. The Si particles were refined to <3 µm, and strength increased from 280 MPa to 350 MPa without losing the ductility (>30%) (Yoon *et al*., 2007). In another study, Swaminathan *et al*. reported the effect of different ECAP processing routes on microstructure refinement, Si particle distribution, and mechanical properties of the Al-7Si alloy (Swaminathan *et al*., 2008). In a recent study, Hosseinzadeh *et al*. employed a novel combination of ECAP and selective laser melting (SLM) on Al-12Si alloy to get better mechanical properties. The tensile strength, yield strength, and elongation were enhanced to 56%, 11%, and 55%, respectively, after four ECAP passes (Hosseinzadeh *et al*., 2021). However, the main objective of the ECAP process is still to get a uniformly distributed microstructure in the different metals and alloys. The major issue of the ECAP process is the service life of the die, which involves complex procedures. More research is needed to improve the output and die quality of the method.

The high pressure torsion (HPT) technique is also a popular SPD method for producing UFG materials by applying a combination of high hydrostatic pressure and shear deformation using a rotational anvil. In this technique, a metal disc of ~1mm thickness and 10mm diameter is usually kept inside the anvil cavity and subjected to high pressure with shear deformation by rotating the anvil. In the shear deformation, the equivalent strain (ε_{eq}), which is a function of sample radius (r) and the number of HPT turns (N), is determined in the following way:

During shear deformation, the shear strain (γ) can be calculated by using the following equation (Edalati and Horita, 2016)

$$\gamma = \frac{r\theta}{t}, \tag{2.1}$$

Here, r is the radius of the disc-type sample, $\theta = 2\pi N$ is the rotational angle in radians, N is the number of turns, and t is the thickness of the sample. Further, the equivalent strain (ε_{eq}) is calculated by using the following equation

$$\varepsilon = \frac{\gamma}{\sqrt{3}} = \frac{2\pi N r}{\sqrt{3}t}, \tag{2.2}$$

The HPT technique was first developed by Bridgman in 1935. He studied hundreds of materials under the HPT process and was mainly interested in investigating the polymorphic phase transformations (Bridgman, 1935). Valiev *et al*. reported that the submicron-size grains in Al alloy were made using the HPT technique in 1988 (Valiev *et al*., 1988). In another study, Zhilyaev *et al*. investigated the effect of HPT in commercial-purity aluminium and reported a variation in grain size from the centre (1μm) to the edge (1.2-1.5μm) as well as the hardness variation of the disc-type sample after four HPT turns (Zhilyaev *et al*., 2005). The microstructure and hardness were found to be homogeneous as a function of radius after eight HPT turns. Islamgaliev *et al*. studied the structural features of commercial purity silicon processed by the HPT technique (Islamgaliev *et al*., 1999). Lee *et al*. conducted research on the effect of HPT on the microstructural refinement and mechanical properties of Al-3Mg alloy. Significant grain refinement was obtained from an initial grain size of ~830μm to the final grain size of ~180-190nm up to 10 HPT turns. Initially, grain size decreases abruptly with increasing HPT turns or equivalent strain and then saturates with increasing HPT turns, Figure 2.8(a) (Lee *et al*., 2016). Also, hardness variation with sample radius or equivalent strain has been observed in Al-3Mg and A7075 aluminium alloys after HPT and HPT combined with ECAP. The hardness is minimal at the centre and maximal at the edge of the sample, Figure 2.8(b,c) (Sabbaghianrad, Kawasaki and Langdon, 2012; Sabbaghianrad and Langdon, 2014; Lee *et al*., 2016). Edalati *et al*. investigated the variation in hardness as a function of equivalent strain for FCC and HCP metals and reported that low melting point metals such as Zn, Mg, Al show flow softening during HPT processing, whereas FCC metal show flow hardening and then achieve the steady state condition, Figure 2.9(a) (Edalati and Horita, 2011, 2016). It may be affected by the stacking fault energy and homologous temperature of the metals, Figure 2.9(b). Similarly, Cepeda-Jimenez *et al*. reported the variation in dendrite thickness and hardness as a function of HPT turns/strain and distance across the sample diameter of hypoeutectic Al-7Si alloy (Cepeda-Jiménez *et al*., 2014). The same Al-7Si alloy produced by HPT revealed a variety of microstructures for better corrosion resistance (Wang *et al*., 2015). In a recent work on hypoeutectic Al-7Si alloy, Liu *et al*. investigated the nanostructure of Si particles and Al matrix formation within the two-phase system using the HPT technique. The major particles were refined to 3μm from the initial size of 6μm, whereas the Al matrix average size was obtained to 300nm. Also, many nanosized silicon particles of ~10nm were randomly distributed within the Al grains (Liu *et al*., 2021). However, Zhilyaev *et al*. reported the growth of Si particles and Al matrix near the edge of the specimen during the HPT process at room temperature under 6GPa hydrostatic pressure due to localized heating of the sample (Zhilyaev *et al*., 2007). In many other studies, the HPT process was employed for Al-Si alloys (Venkateswarlu *et al*., 2011; X. Zhang *et*

al., 2020; Yusuf, Hoegden and Gao, 2020; Gebril *et al.*, 2022; Maziarz *et al.*, 2022) and other alloys (Dobatkin *et al.*, 2005; Zhilyaev and Langdon, 2008; Loucif *et al.*, 2010; Ghosh, Gao and Starink, 2012; Sabbaghianrad, Kawasaki and Langdon, 2012; Cubero-Sesin, Arita and Horita, 2015; Jahedi, Paydar and Knezevic, 2015; Kawasaki *et al.*, 2016; Mwema *et al.*, 2019) to get the UFG microstructure with a homogeneous distribution of the second phase and better mechanical properties. In addition, most of the previous studies based on Al-Si alloys were reported only for hypoeutectic composition (Al7%Si), and some studies on AlSi10Mg alloys. These studies mainly focused on the refinement of the microstructure and its effect on enhanced mechanical properties. The results of processing by ECAP and HPT gave a grain size of submicron level, and both are comparable, but the processing of disc-type samples by HPT usually leads to producing a gradient microstructure and mechanical properties from the centre to the periphery of the sample, Figure 2.8(b,c).

Over the last two decades and in recent times, the HPT technique has not only been used for producing UFG but also to explore the other features of metals and alloys, like the development of texture (Orlov *et al.*, 2009), phase transformation during SPD (Pérez-Prado *et al.*, 2008), solid-state reactions (Ivanisenko *et al.*, 2003), enhancement in diffusion bonding, high wear resistance (Wang *et al.*, 2012), high corrosion resistance (Faghihi, Li and Szpunar, 2010), superplasticity (Valiev *et al.*, 2010), thermal stability (Popov *et al.*, 2012), thermal and electrical conductivity (Champion *et al.*, 2011), superconductivity (Nishizaki *et al.*, 2013), improved magnetic property (Straumal *et al.*, 2009), shape memory effect (Waitz *et al.*, 2007) and many more.

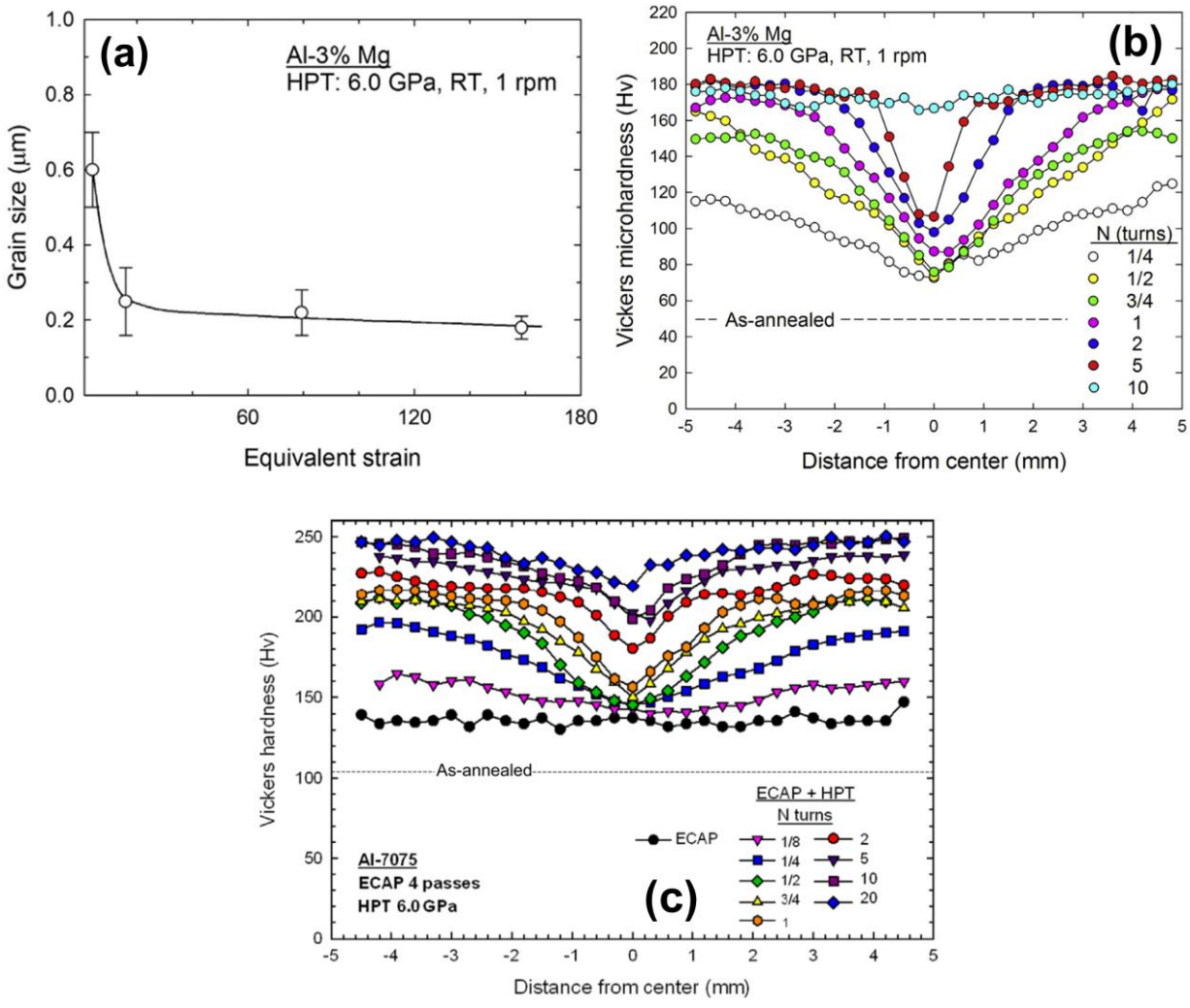


Figure. 2.8 : (a) Variation in grain size as a function of HPT turns, or equivalent strain in Al-3Mg alloy, (b,c) microhardness varies with distance across the sample diameter of Al-3Mg and Al-7075 alloys (*Source*: Sabbaghianrad, Kawasaki and Langdon, 2012; Sabbaghianrad and Langdon, 2014; Lee et al., 2016)

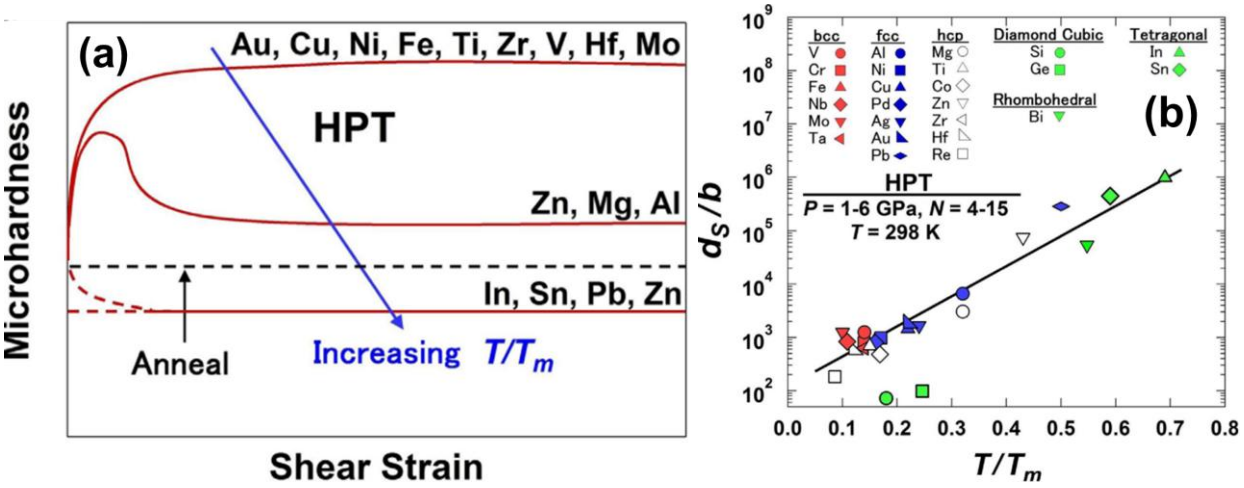


Figure. 2.9 : (a) Plot of microhardness as a function of shear strain showing strain hardening and softening under the HPT process of various pure metals, (b) plot of d_s/b as a function of homologous temperature (*Source*: Edalati and Horita, 2016)

Friction stir welding (FSW) was introduced by the Welding Institute UK in 1991 to make solid-state joining of Al alloys. Later, it was developed as a processing technique called friction stir processing (FSP) by Mishra *et al*. for microstructural modification to get the UFG material and better mechanical properties (Mishra and Mahoney, 2001; Ma *et al*., 2003; Mishra and Ma, 2005). It involves a traverse motion of a rotating tool inside the material, which causes intense plastic deformation. Due to the stirring action of the tool and contact of the tool shoulder and material surface, localized heat generation takes place, which is treated as the thermo-mechanical treatment of the material, causing grain refinement. Some advantages of the FSP process are listed below:

1. It is a solid-state, single-step thermo-mechanical treatment using severe plastic deformation, providing a homogenous microstructure with UFG and a good combination of strength and ductility.
2. The microstructure and property can be controlled through the input parameters, like tool speed, tool geometry, work material, cooling conditions, etc., involved in FSP techniques.
3. It is a green, eco-friendly, and energy-efficient process compared to the other conventional thermo-mechanical processes.
4. It is an emerging technique that has evolved nowadays to explore more experimental work and scientific applications.

Mahoney *et al*. applied FSW to weld the 7075 Al alloy (Mahoney *et al*., 1998), whereas, in the Al-Si alloy, a significant fragmentation of the needle-like coarse Si particle of 27±23μm in the as-cast state to 2.6±2.4μm fine globular Si particles was achieved by the two-pass FSP process as a severe plastic deformation technique (S M Aktarer *et al*., 2015). At the same time, the microstructural refinement enhanced the mechanical properties, such as hardness, which increased from 58HV to 67HV, and yield strength and tensile strength, which increased by 20% and 29%, respectively. Also, three affected regions of the material being processed through FSW were reported: (i) stir zone (SZ), (ii) thermo-mechanical affected zone (TMAZ), (iii) heat affected zone (HAZ), presented in Figure 2.10. There appears to be a microstructure variation in all three zones after FSP, the finest one related to the stir zone. Firstly, Mishra *et al*. investigated the FSP-processed 7075 Al alloy and reported the grain refinement to 3.3±0.4μm along with the deformation behaviour at high temperatures (R.S. Mishra, M.W. Mahoney, S.X. McFadden,

2000). Dynamic recrystallization was reported to be the prominent grain-refinement mechanism during FSP. Other than this, other factors (S. Jana *et al.*, 2010; Tutunchilar *et al.*, 2012) like tool geometry, rotational and traverse speed, alloy composition, heat generation, applied pressure, and cooling conditions were also studied that affect the structure-property interrelationships. Yadav and Bauri showed a significant grain refinement to 3µm from the initial coarse grain size of 84µm in commercially pure Al. It is validated by EBSD and TEM characterization techniques that the dynamic recrystallization and texture variation within the stir zone play an important role in grain refinement and improved mechanical properties (Yadav and Bauri, 2012).

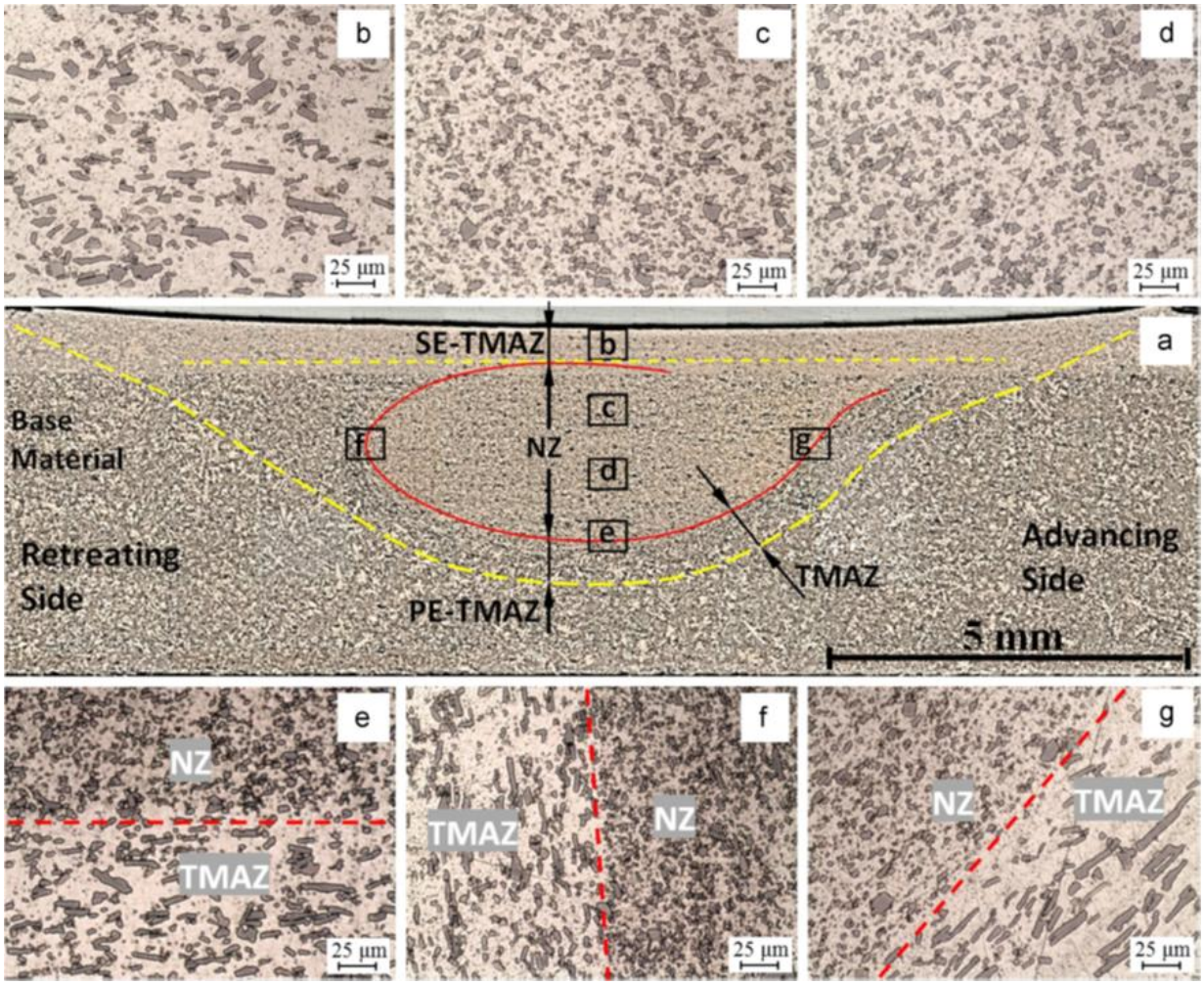


Figure. 2.10 : Macrostructures of different sections marked of FSP processed Al-12Si eutectic alloy (a), also the higher magnified images are taken; the thermally affected zone (TMAZ) (b), nugget zone (NZ) (c,d), combined TMAZ and NZ region from the top surface (e), combined TMAZ and NZ region from the retreating side (f), transition of TMAZ and NZ region from the advancing side (g) (*Source*: S M Aktarer et al., 2015)

The effect of the traverse speed of the tool on the microstructure evolution and mechanical properties of hypoeutectic Al-7Si alloy was investigated by Soleymanpour *et al.* (Soleymanpour, Aval and Jamaati, 2022a). FSP employed at 120mm/min speed was found to be optimum for grain refinement and homogeneity in the particle distribution, which resulted in improved mechanical properties. Beyond this speed, there was a decrease in strength and the formation of cavities. Ma *et al.* applied the FSP to as-cast Al-7Si alloy, which developed the microstructure with fine Si particles of 0.25-0.42µm with homogeneous distribution in the Al matrix of 3-4µm (Ma, Sharma and Mishra, 2006). Recently, a heterogeneous microstructure evolution after three passes of FSP of Al-4Si alloy was reported by Escobar *et al.*, where microstructure evolution occurred due to the particle-stimulated grain nucleation (PSGN), recovery, and dynamic recrystallization. They discussed in-depth characterization by high-energy synchrotron X-ray diffraction, EBSD, and TEM (Escobar *et al.*, 2021). In some studies,

FSP has been applied to improve the strength, ductility, and machinability of the as-cast Al-6.5Si to hard-to-work hypereutectic Al-30Si (Guru *et al.*, 2015; Rao *et al.*, 2015, 2016). Rao *et al.* reported the bimodal ultrafine Si particles and nanosized level Al grains after three passes of the FSP of Al-30Si, which improved the tensile strength by four times and ductility by fourteen times. Cheng *et al.* produced the Al-7Si alloy and optimized the mechanical properties by combining FSP and rolling (Cheng, Liu and Ge, 2021), whereas in another study, Meenia *et al.* investigated the effect of FSP up to three passes with and without pre-process heat treatment on microstructure refinement and mechanical property enhancement in Al-7Si alloy (Meenia *et al.*, 2016). Interestingly, the combined effects of heat treatment, rolling, and FSP were studied by Soleymanpour *et al.* in Al-7Si alloy and reported the best Si morphology with a size of 2.23µm in the FSPed sample. The microhardness (94HV), yield strength (288.7MPa), and tensile strength (296MPa) were obtained to be maximum in the rolled sample, Figure 2.11 (Soleymanpour, Aval and Jamaati, 2022a). Overall, the FSP technique is a very suitable method to produce UFG, defect-free alloy and materials with higher mechanical properties without any harmful effects on the environment.

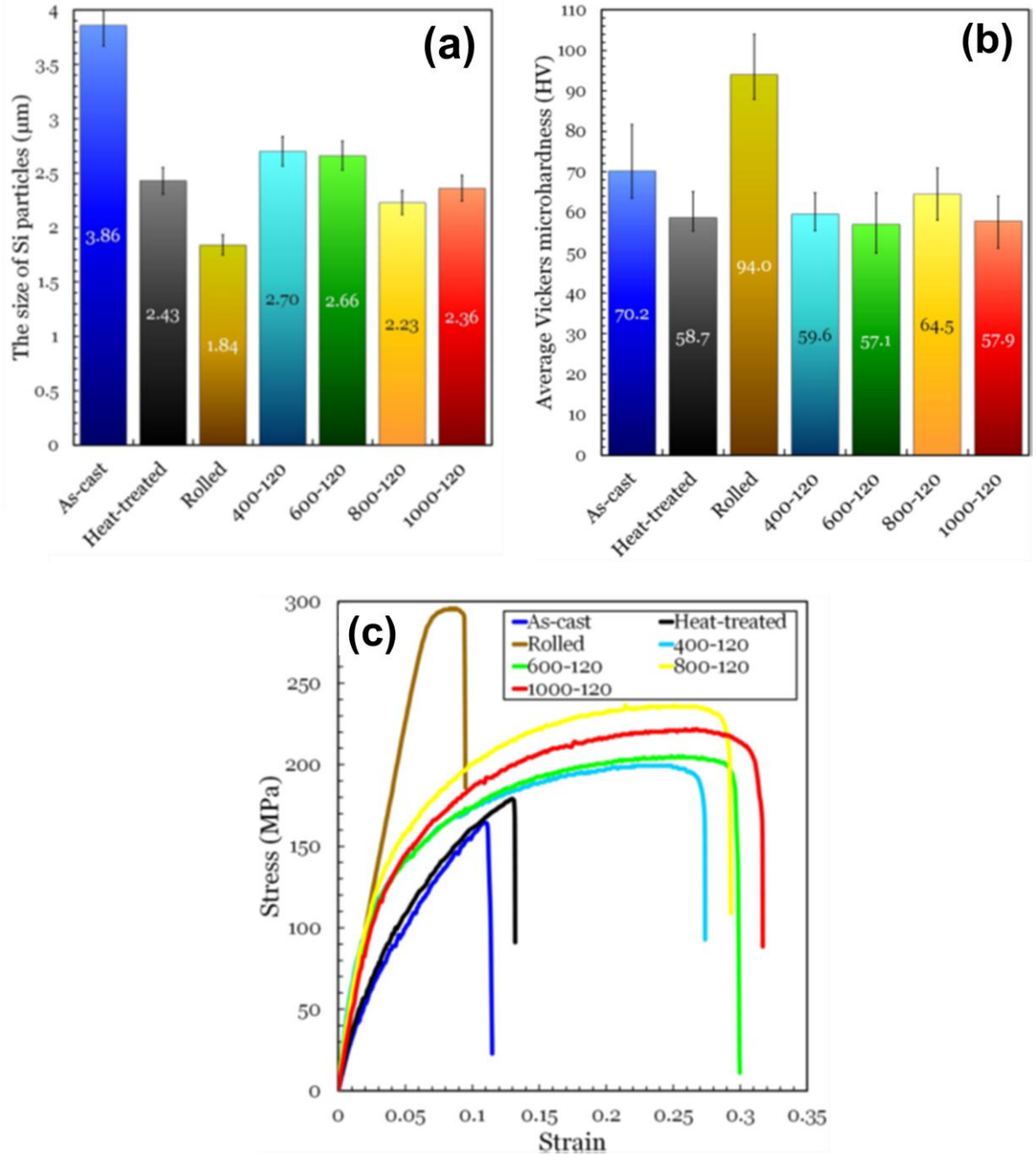


Figure. 2.11 : Variation in Si particle size (a), microhardness (b), yield strength, and tensile strength (c) as a function of process conditions (*Source*: Soleymanpour, Aval and Jamaati, 2022)

Other than this, in a very recent study, Choudhary *et al*. investigated the effect of multi-direction forging (MDF) on the changes that occurred in microstructural and mechanical properties of hypereutectic Al-16Si and Al-20Si alloys (Choudhary *et al.*, 2024). They reported that higher hardness, tensile strength, and ductility were obtained for the samples that were refined after MDF.

A comparison of the micrographs obtained from HPT, ECAP, and FSP has been made to illustrate the effect of the SPD process on the refinement level and distribution of the phases, shown in Figure 2.12(a-d). All the processes show approximately the same results. Interestingly, Kashyap and Telang used the explosive working method for grain refinement of Pb-Sn alloy, which also resulted in a microstructure quite similar to that obtained from other severe plastic deformation techniques. The concentric circles formed in Figure 2.12(d) (Kashyap and Telang, 1991) are especially noted to be similar to those reported in the centre region of samples that have undergone HPT (Wilches Pena *et al.*, 2021).

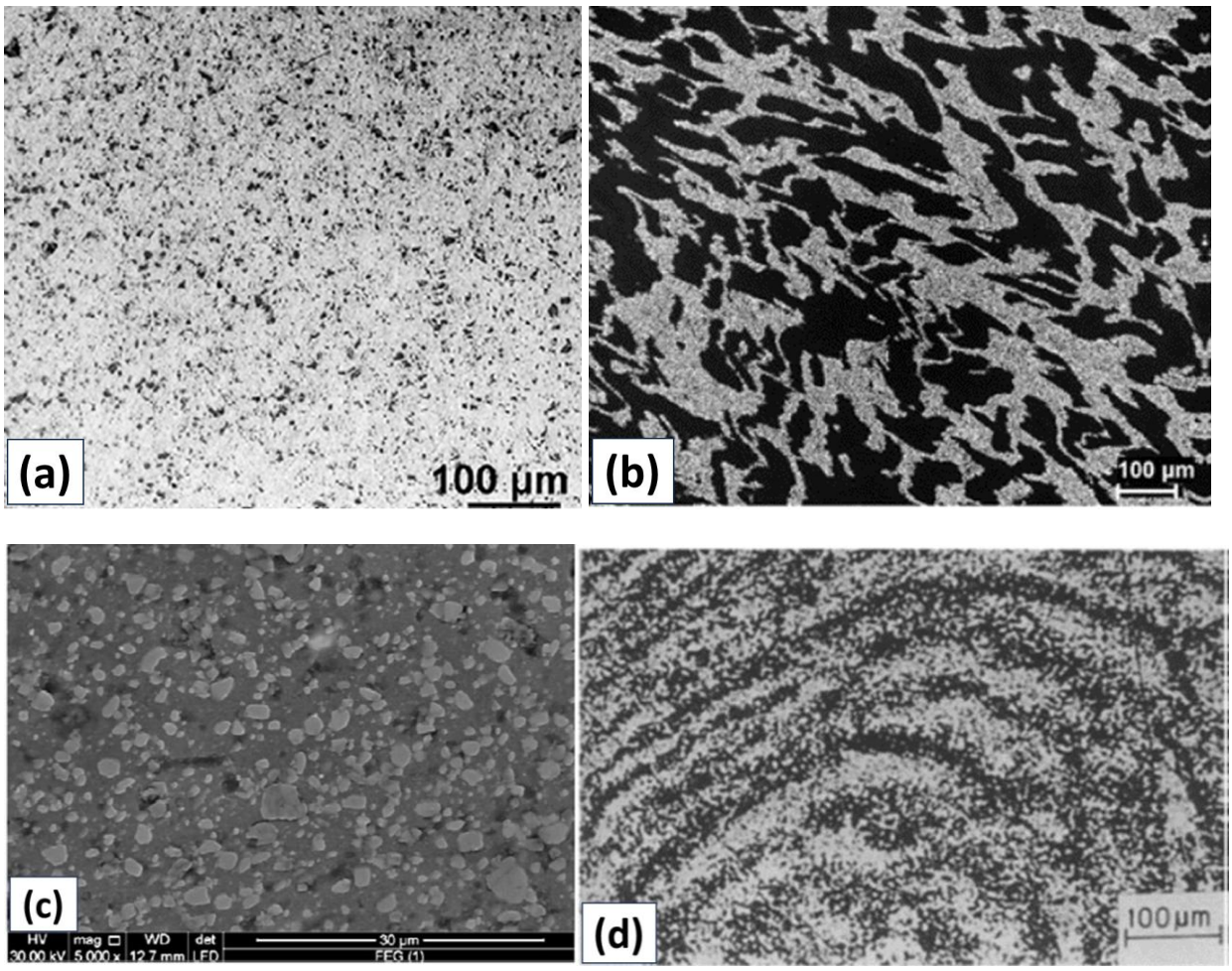


Figure. 2.12 : (a) Optical microstructure of HPT processed (*Source*: Liu et al., 2021), (b) SEM SE micrograph of 8 pass ECAP (*Source*: García-Infanta et al., 2010), and (c) FSP processed Al-7Si alloy (*Source*: Mahmoud, 2013), (d) micrograph of the deformed Pb-Sn alloy by Explosive forming (*Source*: Kashyap and Telang, 1991)

2.4 DEFORMATION BEHAVIOR OF THE METALS AND ALLOYS

The deformation behaviour of any metal and alloy talks about the response of the materials to an externally applied load or strain rate. If the applied load goes beyond the threshold strength, called yield strength, the material undergoes plastic deformation. The

nature of the stress-strain curve represents the deformation behaviour of the materials. The deformation involves the following steps, which can be related to the stress-strain curve as well:

I. Activation of slip systems
II. Initiation of dislocation generation and motion at low strain level,
III. Dislocation-dislocation interaction causing its accumulation at higher strain,
IV. Strain hardening
V. Attaining peak stress and further start of necking
VI. Fracture

Deformation behaviour or the nature of the stress-strain curves differs among different materials, and it depends on material composition, processing variables, crystal structure, structures at different length scales, and test conditions like strain rate (or stress in the case of creep) and test temperature. Here, the work is limited to binary two-phase Al-Si alloys, their processing, and deformation behaviour at ambient and high temperatures by using constant strain rate (cross-head speed) type tests. Therefore, the literature to be followed below will be focused on such relevant aspects of deformation.

The nature of flow stress is affected by the homologous temperature (T_m) of the material. At low homologous temperature (Region-I, $T \leq 0.25T_m$), the yield strength decreases with increasing temperature, and the work hardening is associated with the short-range barrier to dislocation motion (D. Hull and D. J. Bacon, 2011). At intermediate homologous temperature (Region-II, $T \sim 0.25$ to $0.7T_m$) the yield strength is generally independent of temperature owing to long-range obstacles to dislocation motion (Courtney, 2009). However, there comes a deviation in the nature of temperature dependence of increasing strength in the presence of dynamic strain aging. At high homologous temperature (Region-III, $T \geq 0.7T_m$), the yield strength decreases with increasing temperature by virtue of temperature-assisted deformation through diffusional contribution. For low melting point metals like Pb, Sn, and Zn, the room temperature will be considered as a high homologous temperature. As the homologous temperature increases, the rate of work hardening/flow stress decreases, and elongation increases. However, at high homologous temperatures ($>0.7T_m$), the grain boundary sliding and diffusion control the deformation process. A decreasing temperature and increasing strain rate show a similar trend of variation in strength, and as such, the yield strength increases with increase in strain rate and decrease in temperature. The nature of the stress-strain curve depends on both temperature and strain rate. Generally, there occurs work hardening at lower temperatures, but the temperature dependency of flow stress, including the ultimate tensile strength, retains the same trend of variation as noted for the yield strength with temperature above. There exist different theories of work hardening as published in several classical papers and books (Koehler, 1952; Kocks, 1966; Kuhlmann-Wilsdorf, 1985; Kuhlmann-Wilsdorf and Hansen, 1989; Rollett and Kocks, 1993). The stress-strain curves in the presence of work hardening and dynamic recovery exhibit several stages of work hardening rate (θ) vs. stress (or strain) plot. They are summarized with increasing stress (strain) into five stages as (i) increase in θ (stage I), (ii) steady state (no change in θ, stage II), (iii) linear decrease in θ (stage III), (iv) second steady state (no change in θ, stage IV), and (v) mild decrease in θ (stage V). These stages in pure Ni and Ni-Cr alloys were explained to arise from the transition of elastic to plastic region, formation of dense planar slip bands, and gradual decrease in rate of dislocation density, respectively (Zhang, Han and Li, 2021). At high temperatures, the nature of stress-strain curves widely varies as influenced by a combination of several high-temperature phenomena and mechanisms to be presented later.

2.4.1 Room Temperature Deformation of Metal and Alloys

The primary mechanisms governing plastic deformation in metals and alloys at room temperature involve slip systems, dislocation activities, and, in certain instances, twinning. Specifically, plastic deformation in HCP metals primarily occurs through twinning (Cao *et al.*,

2018; Hama, 2020), while in high stacking fault energy FCC metals like Al, deformation is primarily driven by slip systems with dislocation motion, and twinning is negligible. In polycrystalline materials, dislocation motion is impeded by grain boundaries, leading to dislocation accumulation near these boundaries. Consequently, dislocation-dislocation interactions occur, hindering the dislocation motion. Dislocations either pile up or traverse the grain boundaries depending on the applied load (macroscopically) and the grain orientations (microscopically). Pile-ups strengthen the material by impeding dislocation movement, a phenomenon known as strain hardening or work hardening. Kuhlmann-Wilsdorf elaborated on the theory of work hardening, tracing its evolution from early theories like Orowan's (Humphreys and Hirsch, 1976) to its contemporary understanding (Rollett and Kocks, 1993), which encompasses various stages of work hardening in different metals and alloys (Kuhlmann-Wilsdorf, 1985). Furthermore, if the material undergoes localized straining due to stress concentration at a point in the material, it leads to neck formation and ultimate failure.

However, in two-phase materials, the deformation behaviour depends on several factors, including the phase constituents, phase fractions, phase morphology, and physio-mechanical properties of each phase (Ankem *et al.*, 2006). Moreover, the mechanical properties of individual phases, such as hardness, strength, and ductility, significantly influence the overall deformation characteristics of the alloy. The phase compatibility and deformation in a coordinated manner of the phases led to the extension of the failure of the alloy. The plastic deformation of a two-phase material is considered non-homogeneous (Ashby, 1966) because it would not be possible to deform them equally. One of them (matrix phase) can exhibit more ductility, and the other is harder (particles). In the deformation process, the ductile phase deforms more than a harder phase, which creates a gradient of deformation within the alloy microstructure, and geometrically necessary dislocations (GND) fill this gap, as shown in Figure 2.13. Thus, these stored GNDs are responsible for the work hardening of the two-phase alloys.

Yegneswaran and Tangri studied the deformation behaviour of two-phase Cu-Al alloys at room temperature and explained the effect of the second phase on the flow stress, work hardening, and total elongation (Yegneswaran and Tangri, 1984). The flow stress and work hardening of the alloys increased with an increase in the fraction of the second phase, whereas the elongation decreased with an increase in the second phase fraction. In another study, Prasad Rao and Tangri studied the deformation behaviour through compression tests at room temperature of titanium aluminides by varying the phase proportions (Prasad Rao and Tangri, 1992). They reported that the microcrack forms due to the decohesion of phases, which promotes the ultimate failure of the alloys. A model was developed by Poech and Fischmeister to explain the deformation behaviour of two-phase materials (Poech and Fischmeister, 1992). This model focuses on the strain compatibility of both phases, which includes the stress triaxiality caused by a hard response of the softer phase and a soft response of the hard phase, which was validated with the experimental results of the WC-Co two-phase alloy. In another study, Neti *et al*. reported the finite element simulation results on the variation of stress-strain behaviour by varying the volume fraction of the second phase from 20% to 80% (Neti, Vijayshankar and Ankem, 1991). Similarly, Ankem *et al*. investigated the deformation behaviour of two-phase (α+β) Ti alloy (Ankem, Joost and Schwarm, 2019), and Feng *et al*. reported the same results by investigating the deformation behaviour of two-phase Ti-Al alloy using finite element simulation and molecular dynamic simulation, respectively (Feng *et al.*, 2019). Sherafat *et al*. investigated the deformation behaviour of the two-phase Al/Al7075 alloy fabricated through the hot extrusion process by varying the proportion (%) of Al powder of the specimen (Sherafat *et al.*, 2010). They reported that the work hardening exponent n was found to be a function of the second phase fraction, and the fracture mode changed from ductile to brittle after decreasing the Al fraction from 90% to 40%.

Ravichandran used a simple continuum mechanics model to describe the deformation behaviour of the two-phase composite materials containing a coarse, hard second phase in the

soft matrix (Ravichandran, 1994). The model predicted that the flow stress and work hardening exponent increased with an increase in the volume fraction of the second phase particles, and these results were also verified with the numerical and finite element simulations and with the experimental measurements as well. Stolarz *et al*. studied the deformation behaviour of two-phase Al-Si at room temperature. It is reported that the soft Al matrix is ductile and more deformable, whereas, in contrast, the Si phase is much harder and non-deformable (Stolarz, Madelaine-Dupuich and Magnin, 2001). Due to this incompatibility, the overall mechanical properties are influenced, and the fracture occurs in a mixed or pseudo-brittle type (Tian *et al*., 2011). In some of the more interesting research (Edalati *et al*., 2017; Somekawa *et al*., 2018; Demirtas and Purcek, 2019; P. Liu *et al*., 2019; Nohira *et al*., 2022; Edalati, 2023), the two-phase materials exhibit superplasticity even at room temperature due to the SPD effect and some alloying addition, which causes the grain boundary sliding mechanism to occur at low temperatures.

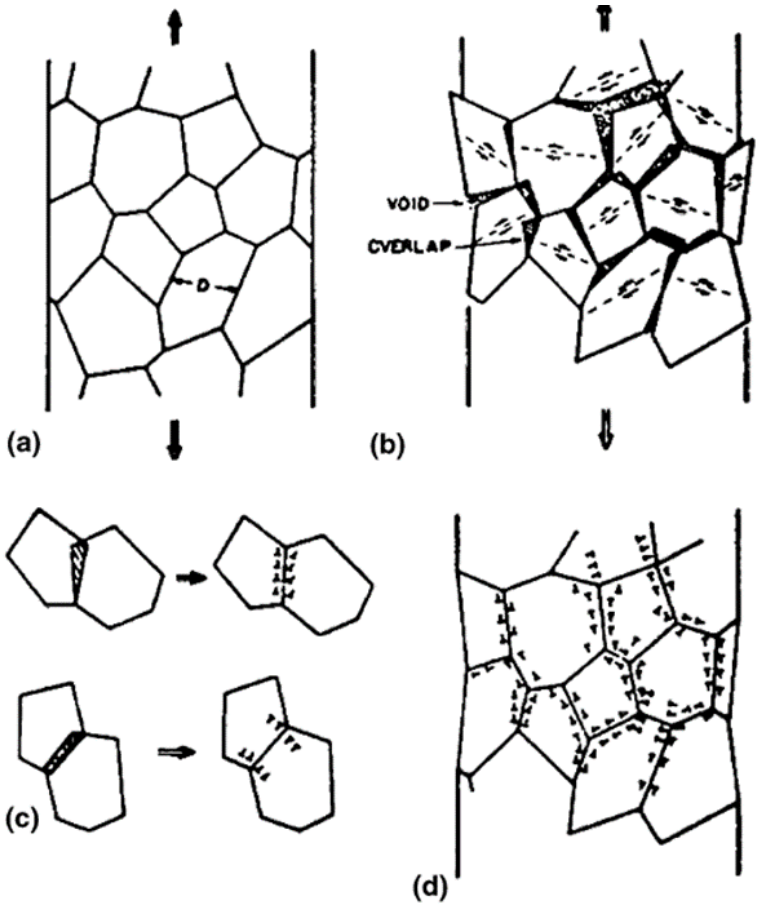


Figure. 2.13 : (a) Schematic figure of anisotropic deformation of polycrystalline material, (b) void formation, (c) gathering of geometrically necessary dislocations, and (d) void filled by GND (*Source*: Courtney, 2009)

(a) Strengthening mechanisms for deformation

Understanding the strengthening mechanism that governs the deformation behaviour of metals and alloys is necessary. The mechanical properties of the alloys depend on the chemical composition and the processing methods involved. Conventional processing methods, such as melting and casting, metal forming methods, and severe plastic deformation methods, are used to enhance strength by contributing in different ways. Material strengthening can be increased by restricting the dislocation movement during deformation. The dislocation motion can be hindered by different types of obstacles, like dislocations themselves, solute atoms, second-phase particles, grain boundaries, and others (Courtney, 2009). Based on this, the possible strengthening mechanisms are listed below:

I. Work hardening (dislocation strengthening): When dislocation-dislocation interaction itself hinders dislocation motion during the deformation, it leads to the strengthening of material requiring higher stress for further deformation. This stress is estimated by the following equation (Kocks, 1966):

$$\Delta\sigma_{dislocation} = \beta M G b \sqrt{\rho_d}, \tag{2.3}$$

where β is the material constant, M is the Taylor factor, G is the shear modulus, b is the Burgers vector, and ρ_d is the dislocation density.

II. Grain boundary strengthening: Grain boundaries play a major role as obstacles to restrict the dislocation motion. In view of this, the dislocation pile-up within the grain on the slip plane against the grain boundary, which separates the other grain by different orientations. Hall-Petch (E. O. Hall, 1951; N.J. Petch, 1953) calculated the strengthening owing to the grain boundary as given below:

$$\Delta\sigma_{H-P} = k/\sqrt{d}, \tag{2.4}$$

where k is the material constant, and d is the grain size.

III. Particle strengthening: The strengthening occurs due to the dispersion of the small particles in the matrix. It depends upon the particle size and volume fraction, particle shape, and interface between the matrix and the second-phase particles (Ashby, 1966; Humphreys and Hirsch, 1976). One example of particle hardening includes the strengthening caused by the precipitation process. The strengthening caused by shearing or cutting of particles by dislocation is expressed by:

$$(\sigma)_{pc} = C_{pc} G \left(\frac{r}{b}\right)^{0.5} f^{0.5} \varepsilon^{1.5}, \tag{2.5}$$

where f is the second phase fraction, and r is the size of the particle. However, when the hard particle is large and cannot be cut by dislocation then hardening comes from Orowan bowing of dislocations around the particles. In this case, the strengthening is expressed by:

$$\sigma_{pb} = \frac{Gb}{L-2r}, \tag{2.6}$$

where L is the effective or mean spacing between the obstacles within the slip plane and r is the particle radius.

IV. Solid solution strengthening: In solid solution strengthening, the solute atom acts as the obstacle to the dislocation motion and improves the yield strength of the alloy. Also, it depends mainly on the mutual effects of size and modulus of the solute and solvent atoms. Fleischer and Labusch estimated the solid solution strengthening by considering the following equation (Fleisgher, 1961; Labusch, 1970):

$$\left(\sigma_y\right)_{ss} = \frac{G\varepsilon_c^{3/2} c^{1/2}}{700}, \tag{2.7}$$

where c is the concentration of the solute atoms.

The above-listed mechanisms contribute to the strength of the metals and alloys by means of dislocation density, grain size, particle size and volume fraction, the concentration of the solute atom, the precipitate size, and finally, the two-phase nature of the alloy.

In Al-Si alloys, work hardening, grain boundary strengthening, and particle strengthening majorly contribute to the strengthening, whereas solid solution strengthening does not significantly affect yield strength. However, Ma *et al*. reported that after the application of high-pressure solidification, solid solution strengthening is the dominating strengthening mechanism in hypereutectic Al-20Si alloy, along with grain boundary strengthening (Ma *et al*., 2016). The solubility of the Si in Al increased from 0.05wt.% to 6.96wt.% as a function of applied pressure up to 3GPa. Liu *et al*. investigated the effect of Si particle refinement on the strengthening of Al-Si alloy and suggested the Orowan mechanism for improving the yield strength (M. Liu *et al*., 2019). Moreover, Takata *et al*. reported the anomalous strengthening by the contribution of nano-sized particles in the matrix in the form of precipitation strengthening (Takata *et al*., 2020). Generally, the contribution of Orowan strengthening was maximum, and dislocation density was observed minimum in Al-Si alloys, whereas the grain boundary strengthening showed an intermediate effect or contribution (Chen *et al*., 2017; Hadadzadeh *et al*., 2018). Apart from these effects, sometimes, the yield strength can be enhanced by the co-clustering of the second phase, which leads to the order-strengthening mechanism (Starink, Cao and Rometsch, 2012).

2.4.2 High-Temperature Deformation of Metal and Alloys

Diffusion, grain boundary sliding (GBS), and dislocation slip are the primary mechanisms involved in the high-temperature deformation of polycrystalline materials. Depending on the testing conditions, deformation at elevated temperatures can be predominantly governed by one mechanism or a combination of these mechanisms. Plastic deformation in polycrystalline materials consistently correlates with the deformation of either individual grains or clusters of grains within the material undergoing deformation. Furthermore, these mechanisms drive deformation and contribute to concurrent changes in the material microstructure. Earlier literature (Mukherjee, 1971; Sherby and Wadsworth, 1989; Zelin and Mukherjee, 1996) proposed and reviewed various mechanisms based on the understanding of flow properties and their correlation with microstructure evolution. Recent studies by other authors have further expanded upon these mechanisms that were proposed earlier.

Stress-strain curves of varying nature can be obtained from high-temperature tensile tests, as depicted schematically in Figure 2.14(a,b). Test conditions and initial microstructure significantly influence the dominance of the hardening, steady-state, and flow softening of the stress-strain curve (Samantaray, Mandal and Bhaduri, 2009). Flow-hardening behaviour in the stress-strain curve is attributed to dynamic grain growth and increasing dislocation density during deformation (Kashyap and Tangri, 1987), while flow-softening behaviour is promoted by continuous dynamic recrystallization and cavitation (Kashyap and Tangri, 1986, 1989; Gourdet and Montheillet, 2003; Sakai *et al*., 2014).

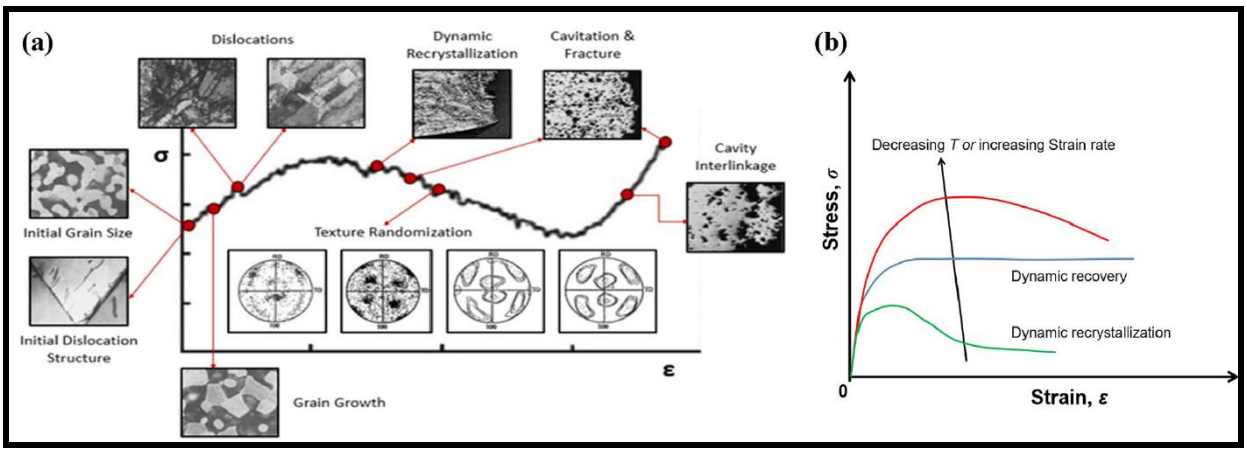


Figure. 2.14 : (a) Schematic stress-strain curve and the corresponding microstructure evolution, (b) effect of strain rate and test temperature on the nature of stress-strain curve (*Source*: Kashyap and Singh, 2022)

Saxena *et al*. devised a processing map to anticipate the deformation characteristics of Zr-1Nb two-phase alloy through innovative methodologies, which incorporate individual phase contributions via microstructural analysis (Saxena *et al*., 2017). Meanwhile, Savaedi *et al*. conducted a comprehensive review of the hot deformation behaviour of high-entropy alloys, proposing constitutive models for flow property prediction (Motallebi, Savaedi and Mirzadeh, 2022). Sakai *et al*. investigated flow curve patterns and concurrent microstructural alterations during high-temperature deformation, encompassing continuous dynamic recrystallization (CDRX), discontinuous dynamic recrystallization (DDRX), geometric dynamic recrystallization (GDRX) (Sakai *et al*., 2014), and grain growth (Huang and Logé, 2016). In the course of high-temperature deformation, dislocations continuously arrange into sub-grains or new cell boundaries (low-angle boundaries) through a recovery process, eventually transforming into high-angle boundaries, forming new grains during the CDRX process (Al-Samman and Gottstein, 2008; Huang and Logé, 2016; Abedi *et al*., 2017). Typically observed in materials with high stacking fault energy (SFE), CDRX contrasts with DDRX, which occurs in low-SFE materials during hot deformation. In DDRX, strain-free grains nucleate and expand at the expense of dislocations. The term GDRX, less explored in literature, describes the recrystallization process in aluminium during high-temperature deformation (McQueen and Kassner, 2004).

Semiatin reviewed the mechanisms operating during thermo-mechanical processing of two-phase Ti alloys and summarized that the flow behaviour was sensitive to phase fraction, morphology, and size of the phases present (Semiatin, 2020). This includes the coarsening of lamella α-phase, spheroidization of Widmanstatten α, substructure formation, and various texture evolutions in two-phase α/β alloys. Similarly, earlier studies examined deformation behaviour in materials such as pure silicon (Korte *et al*., 2011; Kiran *et al*., 2015), pure Al (Puchi and Staia, 1998), Al alloys (Lin *et al*., 2013; Chen, Zhao and Yu, 2015; Khamei, Dehghani and Mahmudi, 2015; Wu *et al*., 2016; Rudnytskyj *et al*., 2020), Mg alloys (Abbasi-Bani *et al*., 2014), high entropy alloys (Cao *et al*., 2020; Abdelghany *et al*., 2022), superalloys (Geng *et al*., 2018), and additively manufactured alloys (Motallebi, Savaedi and Mirzadeh, 2022). These studies often employed Johnson-Cook, modified Johnson-Cook, or Arrhenius models to characterize flow curves contingent upon test conditions and initial and final microstructures. Zamani *et al*. (Zamani *et al*., 2017) and Immanuel and Panigrahi investigated the hot deformation of Al-Si alloys using Johnson-Cook and Arrhenius models for flow curve prediction (Immanuel and Panigrahi, 2018).

(a) Superplasticity in Two-Phase Alloys

Superplasticity is the ability of certain materials to plastically deform several hundred or a few thousand percent without premature failure during tensile tests at high temperatures. The materials show superplasticity if the following conditions or criteria are satisfied (Padmanabhan and Davies, 1980; Sherby and Wadsworth, 1989):

(1) Grain size $d_m \leq 10\mu m$ for metals, and $d_c \leq 1\mu m$ for ceramics;
(2) The shape of the grains should be equiaxed
(3) The nature of the grain boundary structure should be of high angle grain boundary type
(4) Operating temperature should be more than half the absolute melting point, $T \geq 0.5T_m$
(5) The intermediate strain rate falling within the range of, $\dot{\varepsilon}=10^{-5}$-$10^{-2}s^{-1}$, where the strain rate sensitivity of flow stress (m) is ≥0.3.
(6) Superplasticity can be categorized into fine structure superplasticity (FSS) and internal stress superplasticity (ISS).
(7) It can be promoted by having a small size and homogeneous distribution of second-phase particles

Typically, fine-grained polycrystalline materials with grain sizes below 10μm demonstrate enhanced strength at room temperature due to the large number (volume fraction) of grain boundaries (Kim, Estrin and Bush, 2000), which effectively strengthens the material. However, at elevated temperatures, these same grain boundaries facilitate the deformation mechanism known as grain boundary sliding, making the material more susceptible to deformation.

Deformation mechanisms at high temperatures exhibit characteristic trends: the flow stress decreases with rising temperature and decreasing strain rate, and it also diminishes with decreasing grain size. These variations in flow stress concerning temperature, strain rate, and grain size can be quantified using equations such as those formulated by Dorn, Bird, and Mukherjee (J.E. Bird, A.K. Mukherjee, 1969).

$$\dot{\varepsilon} = \frac{AD_0Eb}{kT}\left(\frac{b}{d}\right)^p\left(\frac{\sigma}{E}\right)^n exp\left(\frac{-Q}{RT}\right), \tag{2.8}$$

Here, E is the Young's modulus, b is the Burgers vector, p is the exponent of inverse grain size, n (inverse of strain rate sensitivity index m, n=1/m) is the stress exponent, Q is the activation energy for deformation, k is Boltzmann constant, $D_0\exp\left(\frac{-Q}{RT}\right)$ is the diffusion coefficient, with the terms included having their usual meanings, and A is the material or mechanism-dependent constant.

Ashby and Vernall reported the log (stress)-log (strain rate) plot for high-temperature deformation of lead, which was constructed by taking the data at a wide range of strain rates and temperatures and divided into three regions based on the relative contributions of each mechanism (Ashby and Verrall, 1973). Subsequently, Kashyap and Mukherjee modified the log(σ)-log($\dot{\varepsilon}$) plot and defined all three regions based on the parameters of constitutive relationships for high-temperature deformation of different materials, as shown in Figure 2.15 (Kashyap and Mukherjee, 1985).

Region I: This region is the non-superplastic region, where the values of parameters of constitutive relationships at lower strain rate are m≤0.3, p~2-3, Q~Q_l, and the lattice diffusional creep process is the dominant deformation mechanism.

Region II: This region is termed as superplastic region, where the values of parameters of constitutive relationships at intermediate strain rate are m≥0.3, p~2-3, Q~Q_{gb}, and grain boundary sliding with accommodation by the diffusional or dislocation process is the dominant deformation mechanism.

Region III: Similar to Region I, this region is also the non-superplastic region, but the values of parameters m and Q of constitutive relationships are comparable, viz. m≤0.3, Q~Q_l, but p~0-1. In this region III, the dislocation climb creep process is the dominant deformation mechanism.

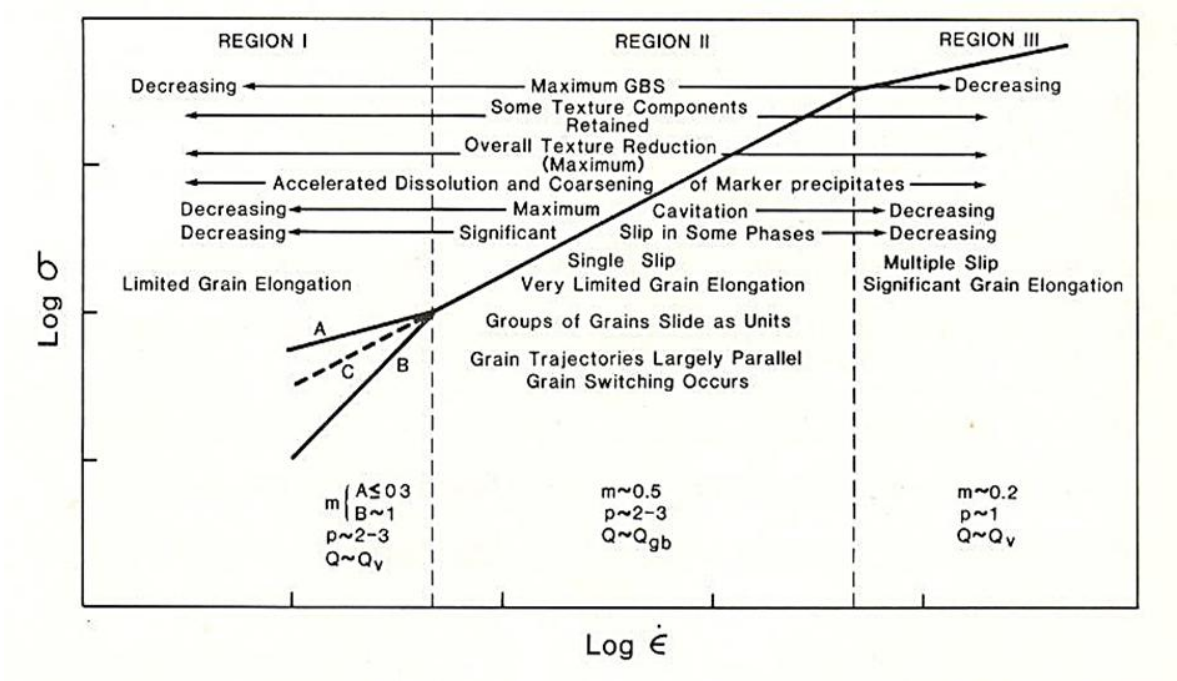
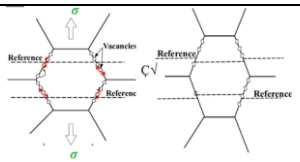
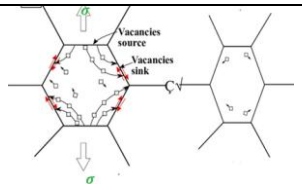
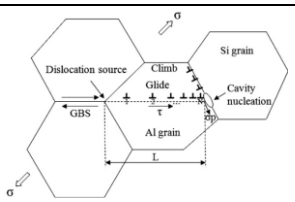
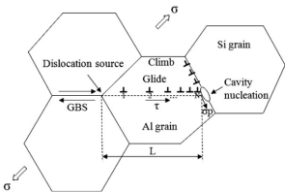
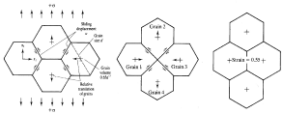
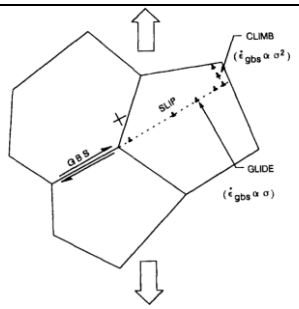
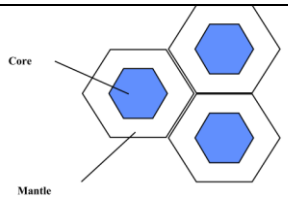


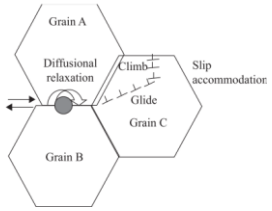
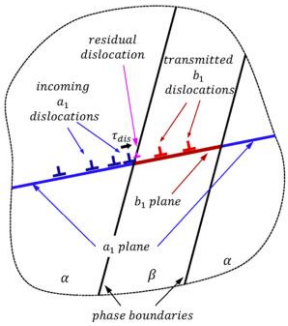
Figure 2.15 : Log (stress) - log (strain rate) plot represents three regions for high-temperature deformation, including superplasticity (region II) and non-superplasticity (region I & III) conditions (*Source*: Kashyap and Mukherjee, 1985)

By considering the values of parameters of the constitutive relationship, various models have been proposed for high-temperature deformation by different authors (Langdon, 1970; Mukherjee, 1971; Ashby and Verrall, 1973; Gifkins, 1976; Gittus, 1977; Sherby and Wadsworth, 1989; Courtney, 2009; Cao *et al.*, 2013; Kassner, 2015; Zheng *et al.*, 2018; Abd-Elaziem *et al.*, 2023), listed in Table 2.2.

Table 2.2 : The list of proposed models along with schematic representations, and suggested values of constitutive relationship parameters

Proposed Model	*Schematic representation*	*Parameters of constitutive relationships*			*Remarks*	*References*
		n = 1/*m*	*p*	*Q*		
Coble creep		1	3	Q_{gb}	Diffusional flow creep occurs at low stress and high temperature.	(Courtney, 2009; Abd-Elaziem *et al.*, 2023)
Nabarro-Herring creep		1	2	Q_l	Diffusional flow creep occurs at low stress and higher temperatures than coble creep.	(Courtney, 2009; Abd-Elaziem *et al.*, 2023)

Grain boundary sliding by lattice diffusion controlled		2	2	Q_l	A transition occurs from the dislocation viscous glide creep into the grain boundary sliding by lattice diffusion mechanism.	(Courtney, 2009; Cao *et al.*, 2013)
Grain boundary sliding by grain boundary diffusion controlled		2	3	Q_{gb}	A transition occurs from the dislocation viscous glide creep into the grain boundary sliding mechanism.	(Courtney, 2009; Cao *et al.*, 2013)
Ashby-Verrall Diffusional accommodation (rate-controlling)		1	2	Q_{gb} to Q_l by considering the effective diffusion coefficient	Grains switch their neighbours and do not elongate much.	(Ashby and Verrall, 1973; Courtney, 2009)
Mukherjee model		2	2	Q_{gb}	Based on GBS and its control by rate of deformation of the grain interior.	(Mukherjee, 1971; Sherby and Wadsworth, 1989)
Gifkins core-mantle model		2	2	Q_{gb}	Grain is divided into core (center) and mantle (peripheral) parts: the GBS and its accommodation by the generation of new dislocations and their climbing along the GB, which are limited to the mantle portion.	(Gifkins, 1976; Kassner, 2015)

Langdon model		2	1	Q_l	GBS occurs by the motion of dislocation and a combination of climb and glide.	(Langdon, 1970; Kassner, 2015)
Gittus model for two-phase materials		2	2	Q_{IPB}	Pileups occur on the dislocation interphase boundaries, and slide-climbs occur from the head of pileups at the IPBs.	(Gittus, 1977; Zheng *et al.*, 2018)

Superplasticity enhances the manufacturing capability of the materials and reduces the time and cost of production. Al and Al alloys are mostly used in the aerospace and automotive industries, where complex parts can be made by using superplastic forming. In the earlier investigations, the study of superplastic deformation of the Bi-Sn alloy was reported by Pearson (Alden, 1967) with elongation of 1950% after the tensile test, but with no failure. In more studies, superplasticity has been obtained in metals and alloys like aluminium, magnesium, titanium, iron-based alloys, nickel-based alloys, and high entropy alloys (Han *et al.*, 2017; Azizi and Mahmudi, 2019; W. Zhang *et al.*, 2019; Bhatta *et al.*, 2020; Nguyen *et al.*, 2020; Al-Hammadi *et al.*, 2023). Initially, superplasticity was achieved by using conventional mechanical processing of the materials, but it was limited to some extent of elongation and for specific materials (Bieler and Mukherjee, 1990; Satoh *et al.*, 1999; W. Kim, Yeon and Lee, 2000; Cao *et al.*, 2013). It was rare to get superplasticity in difficult-to-work materials like HCP metals and magnesium alloys, ceramics, and composite materials (T.G. Nieh, J. Wadsworth, 1997). Now, with increasing interest in SPD techniques (ECAP, FSP, HPT), the development of nano-grained materials has led to improved superplasticity in all types of materials (Kawasaki and Langdon, 2019). Lee *et al*. reported the development of superplasticity in different Al alloys by making use of ECAP as an SPD technique. In most of the Al alloys, the superplasticity occurred at higher temperatures and higher strain rate tests. The maximum elongation of 1680% was obtained at 773K and a strain rate of $10^{-2}s^{-1}$ for Al-Mg-Sc-Zr alloy (Lee *et al.*, 1999, 2002, 2003). Similarly, an exceptional elongation of 4100% was achieved in ECAP-processed Al-Mg-Sc-Zr alloy at 723K and a strain rate of $5.6\times10^{-2}s^{-1}$ (Avtokratova *et al.*, 2012). Ma *et al*. reported the superplastic properties with an elongation >1200% and strain rate sensitivity index (m) of nearly 0.5 in ultrafine-grained FSP processed Al-4Mg-1Zr alloy (Ma, Liu and Mishra, 2010). Also, the superplasticity in Zn-22%Al (1800%) and Al-33%Cu (1200%) was obtained after HPT processing of the alloys (Kawasaki and Langdon, 2014). In some cases, it was obtained at low temperatures, even at room temperature also (Edalati *et al.*, 2017; Somekawa *et al.*, 2018; Demirtas and Purcek, 2019; P. Liu *et al.*, 2019; Nohira *et al.*, 2022; Edalati, 2023). In an interesting study, Edalati *et al*. reported superplasticity in HPT-processed Mg-8Li and Al-Zn alloys at room temperature with elongation of 440%, 480%, and m=0.37, 0.41, respectively (Edalati *et al.*, 2017; Edalati, Horita and Valiev, 2018). The low-temperature superplasticity can be achieved by controlling the grain boundary composition or by changing the α/β phase fraction and the diffusional process of lithium or zinc along the α/α grain boundaries in the above case. The world record maximum superplastic elongation is reported to be 9500% in a Ti-alloy.

The superplasticity of Al-Si alloys has received limited attention in the literature, particularly regarding hypereutectic compositions. Past investigations primarily focused on hypoeutectic Al-Si alloys, with only a handful exploring attempts at hypereutectic

compositions. Notably, earlier work by Satoh *et al*. highlighted the superplastic properties of brittle hypereutectic Al-15Si and Al-25Si alloys fabricated via the P/M route, showcasing impressive elongation percentages of 307% and 154%, respectively, alongside a strain rate sensitivity index (m) exceeding 0.3 (Satoh, Okimoto, Nishida, *et al*., 1995). Chung and Cahoon explored the superplasticity in mechanically processed eutectic Al-13Si alloy at a wide range of temperatures and strain rates. Based on total elongation of more than 300% and the magnitude of constitutive relationship parameters, two mechanisms were dominant: (i) grain boundary sliding and its accommodation at low and intermediate strain rates, and (ii) dislocation climb at high strain rate (Chung and Cahoon, 1979). Also, Kim *et al*. investigated the high-temperature deformation of Al-25Si produced by the spray-forming process and reported superplasticity with a maximum elongation of ~250% (W. J. Kim, Yeon and Lee, 2000). Ma *et al*. investigated the effect of FSP on the high-temperature deformation behaviour of hypoeutectic A356 (Al-7Si) alloy and, for the first time, reported the superplasticity with a maximum elongation of 650% and strain rate sensitivity of 0.45, which suggests the grain boundary sliding mechanism for high-temperature deformation (Ma, Mishra and Mahoney, 2004). Aibin Ma *et al*. and Jing-hua *et al*. studied separately the high strain rate superplasticity in ECAP-processed Al-11Si alloy (Ma, Takagi, *et al*., 2005). The maximum elongation of 192% and strain rate sensitivity of 0.3-0.35 revealed that grain boundary sliding was the dominant mechanism for deformation. In a recent study, superplasticity was obtained in the eutectic Al-12.7Si-0.7Mg alloy processed through the combination of extrusion and rolling process (Cao *et al*., 2013). The maximum elongation of 379% and parameters of constitutive relationship were obtained as m of 0.52 and activation energy for deformation (Q) of 156.7KJ/mol at 793K, which suggests the grain boundary sliding and its accommodation by dislocation slip to be the mechanism for superplasticity.

In summary, the superplastic and non-superplastic deformation mechanisms of the metals and alloys are well presented in the literature. It can be said that the grain boundary sliding along with accommodation by the diffusional process, is the dominant mechanism for superplastic flow, whereas the dislocation climb creep mechanism operates in the non-superplastic higher strain rate region III. However, it may emphasize that no single deformation process can work independently to give superplasticity. In fact, the grain boundary sliding, diffusion, and dislocation slip processes join as leading or accommodating processes depending on the strain rate and temperature conditions, besides the grain boundary phenomena getting affected to facilitate deformation during fine-grained superplastic deformation. Gifkins proposed that the mechanisms for deformation may vary from place to place within the material during superplastic deformation, which indicates the occurrence of micro-scale level heterogeneity during superplastic deformation (Gifkins, 1976).

The cavitation phenomenon happens when the materials deform at high temperatures because of void creation at the triple junction, or sometimes it is related to the second-phase particles (Humphries and Ridley, 1978), if the GBS occurs without being accommodated by other deformation processes. Furthermore, in two-phase materials, the phases that are less probable to diffuse decisively for grain boundary accommodation correspond to the cavitation that occurs during high-temperature deformation (Peterson and Ridley 1981). Mahidhara and Mukherjee observed the cavitation phenomenon in the eutectic Al-Si alloy and reported that the cavity nucleation originated due to grain growth, and the cavity fraction increased with increasing strain (Mukherjee, 1995). Further elaboration of the cavitation is presented in the next section of this chapter.

2.5 METALLOGRAPHIC OBSERVATIONS

The concurrent microstructure evolution during deformation plays a significant role in the flow behaviour of the materials. However, the microstructural evolution depends on the test conditions like strain, strain rate, temperature, and the composition of the materials. At room temperature, the deformation happens due to the movement of the dislocations and,

subsequently, the change in the microstructure, whereas at high temperatures, the dynamic recrystallization, recovery, and grain growth act as the dominant mechanisms for microstructural changes. Moreover, the texture or orientation of the grains has a significant effect on the flow behaviour at room temperature and high temperature as well (Wang *et al.*, 2016; da Silva *et al.*, 2021). Thus, this microstructural evolution controls the deformation behaviour of the materials. Dynamic recrystallization and recovery promote flow softening, whereas grain growth supports the flow hardening behaviour (Ghasemi *et al.*, 2017; Chen *et al.*, 2019). Also, at high temperatures, the dislocation activity is more, which promotes the annihilation or rearrangement of the dislocations, by which the parent grains are converted into sub-grains through the formation of low-angle boundaries (LABs). Further, they can be converted into high-angle boundaries (HABs) by the rotation of sub-grains made from the arrangement of dislocations (Sakai *et al.*, 2014).

Liu *et al*. investigated the effect of temperature on the flow properties and concurrent microstructural changes in Al-Si alloys. The dislocation lines, tangling of dislocations, and substructure formation were observed as a function of temperature and deformation of the alloy, as presented in Figure 2.16(a,b) (Liu et al., 2021), whereas Jaglinski and Lakes reported the cavity formation in hypereutectic Al-Si alloy deformed under constant load creep test, Figure 2.16(c) (Jaglinski and Lakes, 2004).

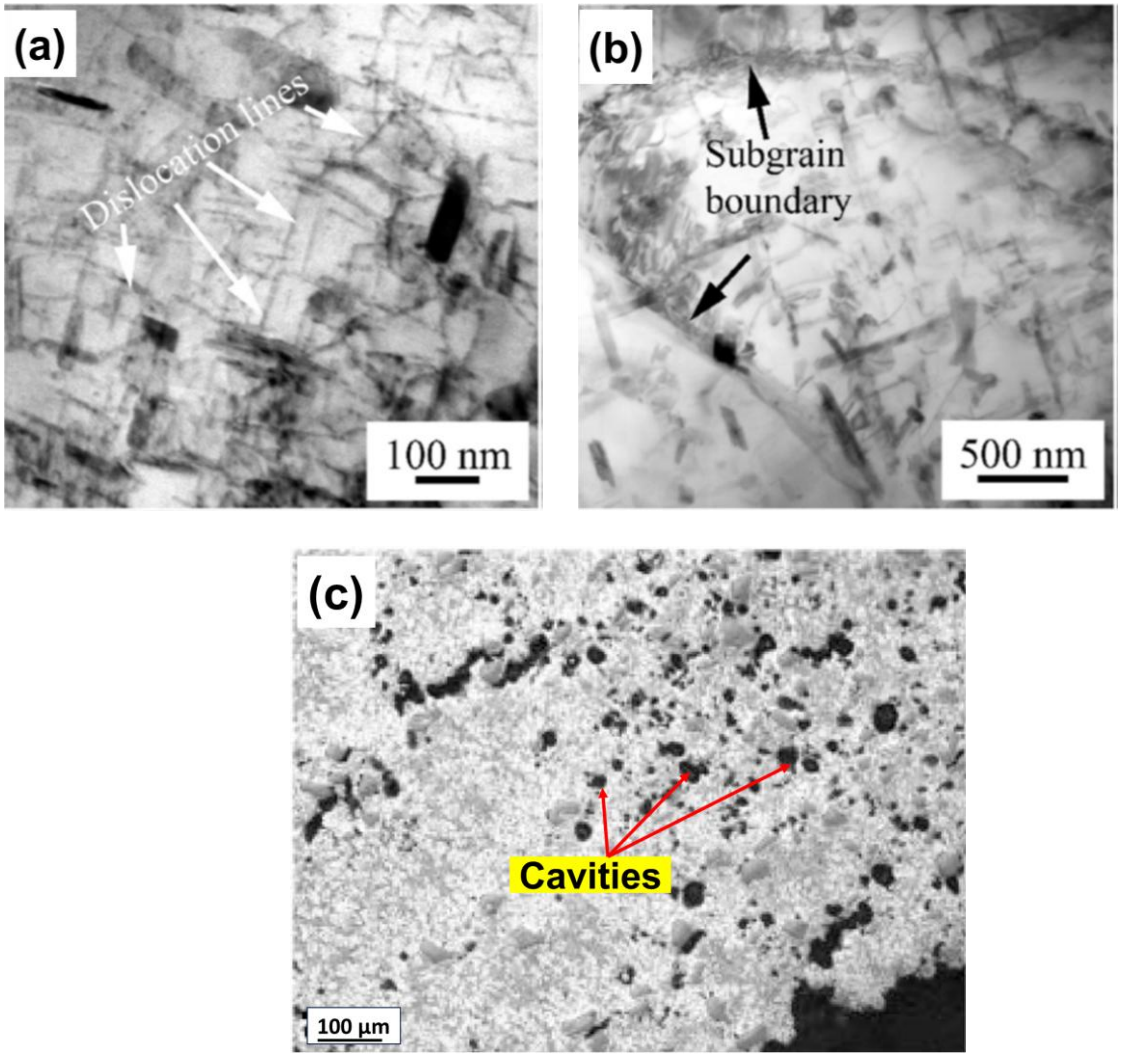


Figure 2.16 : (a-b) Micrographs of the Al-Si alloy after deformation obtained from TEM showing dislocation lines (a), subgrain boundary (b) (*Source*: Liu et al., 2021), and cavity formation in Al-17Si alloy after creep test (c) (*Source*: Jaglinski and Lakes, 2004)

…